Interactions of the Julia set with critical and (un)stable sets in an angle-doubling map on $\mathbb{C}\backslash\{0\}$

Stefanie Hittmeyer, Bernd Krauskopf, Hinke M. Osinga
Department of Mathematics, The University of Auckland
Private Bag 92019, Auckland 1142, New Zealand

December 2013

Abstract

We study a nonanalytic perturbation of the complex quadratic family $z \mapsto z^2 + c$ in the form of a two-dimensional noninvertible map that has been introduced by Bamón, Kiwi, and Rivera-Letelier [arXiv 0508045, 2006]. The map acts on the plane by opening up the critical point to a disk and wrapping the plane twice around it; points inside the disk have no preimage. The bounding critical circle and its images, together with the critical point and its preimages, form the so-called critical set. For parameters away from the complex quadratic family we define a generalised notion of the Julia set as the basin boundary of infinity. We are interested in how the Julia set changes when saddle points along with their stable and unstable sets appear as the perturbation is switched on. Advanced numerical techniques enable us to study the interactions of the Julia set with the critical set and the (un)stable sets of saddle points. We find the appearance and disappearance of chaotic attractors and dramatic changes in the topology of the Julia set; these bifurcations lead to three complicated types of Julia sets that are given by the closure of stable sets of saddle points of the map, namely, a Cantor bouquet, or what we call a Cantor tangle and a Cantor cheese. We are able to illustrate how bifurcations of the nonanalytic map connect to those of the quadratic map by computing two-parameter bifurcation diagrams that reveal a self-similar bifurcation structure near the period-doubling route to chaos in the complex quadratic family.

1 Introduction

We study the dynamics of the two-dimensional noninvertible family of maps

$$\begin{aligned} f : \mathbb{C}\backslash\{0\} &\to \mathbb{C}, \\ z &\mapsto (1 - \lambda + \lambda|z|^2)\left(\frac{z}{|z|}\right)^2 + c, \end{aligned} \tag{1}$$

with $c \in \mathbb{C}$ and $\lambda \in [0, 1]$. For $\lambda = 1$, the family (1) reduces to the well-known complex quadratic family

$$\begin{aligned} f_1 : \mathbb{C} &\to \mathbb{C}, \\ z &\mapsto z^2 + c, \end{aligned} \tag{2}$$

where $c \in \mathbb{C}$ is the only parameter. We are interested in the question of whether, or in which form, the well-known dynamics of the complex quadratic family (2) influences the dynamics of (1) for other values of $\lambda \in [0, 1]$. The main question in this paper is what elements of the dynamics of (2) survive for $\lambda < 1$ and how additional dynamical features appear. This study is in the same spirit as [Bielefeld *et al.*(1993), Devaney(2013), Bruin & van Noort(2004), Blanchard *et al.*(2005), Marotta(2008), McMullen(1988), Peckham(1998), Peckham & Montaldi(2000)], where other perturbations of the complex quadratic family (2) are considered; see Section 2.6 for a brief review of this literature.

The complex quadratic family (2) wraps the plane twice around the origin and translates by c, while the map (1) first opens up the origin to a circle with radius $1-\lambda$, wraps the plane around this circle twice and translates it by c. In particular, (2) is defined on the entire complex plane and every point except c has two preimages, whereas (1) is only defined on the punctured plane $\mathbb{C}\backslash\{0\}$, and only the points outside the circle around c with radius $1-\lambda$ have two preimages. For both maps we call the origin the *critical point* J_0; its image c under (2) is called the *critical value*, and we call the circle around c with radius $1-\lambda$ the *critical circle* J_1 of (1), because it can be thought of as the multivalued image of J_0. The backward iterates of J_0 and the forward iterates of J_1 play a special role in the organisation of the dynamics of (1), and we call them the *backward critical set* $\mathcal{J}^-$ and the *forward critical set* $\mathcal{J}^+$, respectively. Together, they form the *critical set* $\mathcal{J}$; see Section 2.2 for more details. At $\lambda = 1$ in (1), the critical circle J_1 has radius 0 and coincides with the critical value c of (2), and the forward critical set $\mathcal{J}^+$ consists just of the orbit of c accordingly.

Another important difference between the maps (1) and (2) is that (2) is analytic, whereas (1) is nonanalytic for $\lambda \in [0,1)$. In particular, this means that (2) admits only attracting and repelling fixed and periodic points, whereas (1) also allows for the existence of saddle fixed and periodic points, their stable and unstable sets and chaotic attractors. The stable and unstable sets of a saddle point are the generalisations of stable and unstable manifolds for noninvertible maps, that is, they are formed by points that go to a saddle point under forward iteration or that have a sequence of preimages converging to this point, respectively; see Section 2.3 for definitions. As opposed to diffeomorphisms, for a noninvertible map these sets are, in general, not immersed manifolds because the stable set can consist of infinitely many branches and the unstable set may have self-intersections. How do these additional features appear in the dynamics of (1) when $\lambda \in [0,1]$ is decreased from $\lambda = 1$?

The main ingredient in the dynamics of the complex quadratic family (2) is the *Julia set*. It can be defined as the boundary of the basin of attraction of infinity, and we extend this definition to the map (1); see already Section 2.5. The connectivity of the Julia set in (2) is governed by a fundamental dichotomy: it is connected if the orbit of the critical value c is bounded, and it is totally disconnected if this orbit goes to infinity. This dichotomy is encoded by the *Mandelbrot set*, which is the set of parameter values c, for which the corresponding Julia set of (2) is connected; more details are given in Section 2.4. When considering the family (1) with $\lambda < 1$, the orbit of c is replaced by all orbits in $\mathcal{J}^+$, which allows for an intermediate case, where some orbits in $\mathcal{J}^+$ stay bounded and other orbits in $\mathcal{J}^+$ go to infinity. What does this mean for the properties of the Julia set of (1)?

The map (1) is a subfamily of the more general family of maps

$$\begin{aligned} f : \mathbb{C}\backslash\{0\} &\to \mathbb{C}, \\ z &\mapsto (1-\lambda+\lambda|z|^a)\left(\frac{z}{|z|}\right)^2 + c, \end{aligned} \tag{3}$$

with $c \in \mathbb{C}$ and $a, \lambda \in (0,1)$. This map was introduced by Bamón, Kiwi and Rivera-Letelier [Bamón et al., 2006], who kept $c = 1$ fixed. For a, λ both sufficiently close to 1 and for $c = 1$, these authors proved the existence of a *wild Lorenz-like attractor* in this map. A Lorenz-like attractor is a higher-dimensional analogue of the geometric Lorenz attractor [Afrajmovich *et al.*(1977), Afrajmovich *et al.*(1983), Guckenheimer(1976), Guckenheimer & Williams(1979)] in a three-dimensional vector field. More specifically, the Lorenz-like attractor in [Bamón *et al.*(2006)] is constructed in a vector field of dimension $n \geq 5$. It contains an equilibrium with two unstable, one strong stable and $n-3$ weak stable eigenvalues, such that the strong stable eigenvalue dominates the unstable one and the unstable eigenvalue dominates the weak stable ones. Its Poincaré return map on a $(n-1)$-dimensional Poincaré section admits a strong stable foliation and the quotient map of the Poincaré return map on the leaves of this foliation is the two-dimensional noninvertible map (3), which describes the dynamics on the attractor in the underlying n-dimensional vector field. This Lorenz-like attractor is called *wild*, because it contains a hyperbolic set that admits robust homoclinic tangencies, that is, there are C^1-open sets of parameters such that the corresponding hyperbolic set has a tangency between its stable and unstable manifolds. We refer to the existence of a wild hyperbolic set as *wild chaos*.

In [Hittmeyer *et al.*(2013)], we introduced the parameter $c \in \mathbb{C}$ to the map (3) and studied the bifurcations of the stable, unstable, forward critical and backward critical sets as the parameters are moved from the nonchaotic to wild chaotic parameter regime for $a, \lambda \in (0, 1)$; see also [Osinga *et al.*(2013)]. We found that the following four types of tangency bifurcations play a crucial role in the transition to wild chaos:

1. The *homoclinic tangency*, where the stable and unstable sets of a saddle fixed point are tangent;

2. The *forward critical tangency*, where the stable set of a saddle fixed point is tangent to the forward critical set $\mathcal{J}^+$;

3. The *backward critical tangency*, where a sequence of points in the backward critical set $\mathcal{J}^-$ lies on the unstable set of a saddle fixed point;

4. The *forward-backward critical tangency*, where a sequence of points in the backward critical set $\mathcal{J}^-$ lies in the forward critical set $\mathcal{J}^+$.

Homoclinic tangencies are also encountered in diffeomorphisms, but the three critical tangency bifurcations are new and specific to this type of noninvertible map. What role do these four tangency bifurcations play in the dynamics of the map (1) near $\lambda = 1$?

In order to study these questions, we compute the phase portrait of the map (1) for different fixed values of $c \in \mathbb{R}$ and decreasing values of $\lambda \in [0, 1]$, starting with the phase portrait of (2) at $\lambda = 1$. For these phase portraits we compute the fixed and periodic points up to a certain period, their stable and unstable sets, the critical set and the Julia set. Note that (1) is orientation preserving for $c \geq 0$ and orientation reversing for $c < 0$. In Section 3 we choose c in the interior of the Mandelbrot set; more precisely, we choose c in the interior of the *main cardioid*. Here, the complex quadratic family (2) admits an attracting fixed point, which attracts the orbit of the critical value c. When we switch on the perturbation by decreasing λ, we find that the dynamics of (1) for λ sufficiently close to 1 is qualitatively the same as that of (2). More specifically, the radius $1 - \lambda$ of J_1 is small and all the orbits of points on the critical circle J_1 are attracted by the attracting fixed point; the Julia set is a *Jordan curve*, that is, a simple closed curve, and it bounds the basin of attraction of this attractor. However, as λ decreases further, first saddle periodic points appear in pitchfork and period-doubling bifurcations and the dynamics is then organised by their stable and unstable sets. As λ decreases further, we find the tangency bifurcations listed above, but now the different invariant sets also interact with the Julia set. In particular, we find an infinite sequence of forward-backward critical tangencies, which leads to the appearance of infinitely many saddle points; their closure forms a chaotic attractor, which disappears when it interacts with the Julia set in a saddle-node bifurcation. After this bifurcation the Julia set is given by the closure of the stable sets of the saddle points. More precisely, depending on whether the critical point J_0 lies inside the disk bounded by the critical circle J_1 or not, the Julia set has different topological properties. In the former case, the Julia set is a *Cantor bouquet*, that is, a set of infinitely many arcs that emanate from a single point, called an *explosion point*; see also Section 3.2. The latter case leads to a set that also has infinitely many arcs, but now there are infinitely many explosion point; we refer to this set as a *Cantor tangle* and provide more details and a precise definition in Section 3.3. We remark, here, that Cantor bouquets have been found before in maps other than the complex quadratic map [Aarts & Oversteegen(1993), Bula & Oversteegen(1990), Devaney & Krych(1984), Krauskopf & Kriete(1998), Mayer(1990)], but this is the first example of a Cantor bouquet for which the explosion point is finite.

We then consider in Section 4 the case that c is in the exterior of the Mandelbrot set. There, the complex quadratic family (2) has no attracting fixed or periodic point, the orbit of the critical value c goes to infinity and the Julia set is totally disconnected. For λ sufficiently close to 1 in the map (1), there is still no attractor, all the orbits of points on the critical circle J_1 go to infinity and the Julia set is still totally disconnected. As λ decreases, we find a first interaction of the forward critical set J^+ with the Julia set, which is accumulated by an infinite sequence of forward-backward critical tangencies leading to the birth of infinitely many saddle points. After this bifurcation the Julia set is again given by the closure of the stable sets of the saddle points and is a Cantor tangle. As λ decreases further, a first attractor appears in a Neimarck–Sacker bifurcation and the Julia set bounds components of the basins of both the finite attractor and infinity. We refer to this type of Julia set as a *Cantor cheese*; see Section 4.

In order to find out how the transitions for the different values inside and outside the Mandelbrot set are connected, we continue the respective bifurcations in the two parameters $\mathrm{Re}(c)$ and λ. We find that the bifurcation curves emanate from bifurcation points on the boundary and in the interior of the Mandelbrot set. We detect curves of first homoclinic and first backward critical tangencies that lie very close together, and a nearby accumulating sequence of forward-backward critical tangencies, that explains the sudden appearance of infinitely many saddle points and the dramatic changes in the topology of the Julia set over a small parameter range. Furthermore, we find that this bifurcation structure near the main cardioid repeats along the period-doubling route to chaos on the line $\lambda = 1$.

This paper is organised as follows. In Section 2 we discuss the basic properties of the maps (1) and (2) and define the critical, (un)stable and Julia sets for (1). In Section 3 we study the transition of the phase portrait of map (1) for c in the interior of the Mandelbrot set. We start with the special case $c = 0$, where the critical point J_0 is a super-attracting fixed point, and then consider $c = 0.1$ and $c = -0.25$, which represent the orientation preserving and reversing cases in (1), respectively. We discuss the transition for c outside the Mandelbrot set in Section 4 for the representative value $c = 0.28$. In Section 5 we present and discuss the bifurcation diagram in the $(\mathrm{Re}(c), \lambda)$-plane for $\mathrm{Im}(c) = 0$. We end with conclusions in Section 6, where we also extend the fundamental dichotomy of (2) to the map (1) for $\lambda \in (0, 1)$.

2 Notation and Definitions

The map (1) has several properties that are straightforward to derive. Here, we collect these properties, provide the definitions of the critical set and of the stable and unstable sets, recall the basic facts of the complex quadratic family (2), and extend the notion of the Julia set to the map (1) for $\lambda < 1$. A brief overview over the literature on perturbations of (2) is also provided.

2.1 Basic properties of the map (1)

The map (1) maps the punctured plane $\mathbb{C}\backslash\{0\}$ outside the disk $\overline{\mathbb{D}}_{1-\lambda}(c)$ in a 2-to-1-fashion, where $\overline{\mathbb{D}}_r(z)$ denotes the closed disk with radius $r > 0$ centred at $z \in \mathbb{C}$. Therefore, the points in $\overline{\mathbb{D}}_{1-\lambda}(c)$ have no preimages and every point in $\mathbb{C}\backslash\overline{\mathbb{D}}_{1-\lambda}(c)$ has two preimages. For all $c \in \mathbb{C}$ the map (1) is symmetric under rotation by π and for $c \in \mathbb{R}$ it is also symmetric under complex conjugation. The *first preimage* f_0^{-1} is the preimage in the upper half plane or the positive real line, whereas the *second preimage* f_1^{-1} is the preimage in the lower half plane or the negative real line. For $z \in \mathbb{C}\backslash\overline{\mathbb{D}}_{1-\lambda}(c)$, they are given by

$$\begin{aligned} f_0^{-1}(z) &= +\left(\frac{|z-c|-1+\lambda}{\lambda}\right)^{1/a}\sqrt{\frac{z-c}{|z-c|}} \quad \text{and} \\ f_1^{-1}(z) &= -\left(\frac{|z-c|-1+\lambda}{\lambda}\right)^{1/a}\sqrt{\frac{z-c}{|z-c|}}. \end{aligned} \tag{4}$$

The kth preimage $f^{-k}(z)$ of z consists of up to 2^k points; each of these points is given as a sequence of preimages

$$f^{-k}_{s_k \cdots s_1}(z) := f^{-1}_{s_k} \circ \cdots \circ f^{-1}_{s_1}(z),$$

for $(s_l)_{1\leq l\leq k} \in \{0,1\}^k$.

Note that, if we decrease $\lambda \in [0, 1]$ all the way to $\lambda = 0$, map (1) reduces to

$$\begin{aligned} f_0 : \mathbb{C}\backslash\{0\} &\to \mathbb{C} \\ z &\mapsto \left(\frac{z}{|z|}\right)^2 + c. \end{aligned} \tag{5}$$

The map f_0 maps the entire punctured plane $\mathbb{C}\backslash\{0\}$ onto the critical circle $J_1 = \partial\overline{\mathbb{D}}_1(c)$. The points on J_1 have infinitely many preimages, whereas the points in $\mathbb{C}\backslash J_1$ have no preimages; see Section 3.1. For $c = 0$, the map (5) restricted to the unit circle is the angle-doubling map. This map is transitive and the repelling periodic points are dense in the unit circle. If c is varied and $|c| < 1$, the restriction of (5) to J_1 still appears to be transitive and repelling periodic points seem to be dense in J_1, but we did not investigate this in detail. The repelling periodic points of the restriction (5) to J_1 are (degenerate) saddle periodic points of the two-dimensional map (5).

For $\lambda > 1$ and $\lambda < 0$, the dynamics of (1) are more complicated. The origin has infinitely many preimages and every other point inside the disk $\overline{\mathbb{D}}_{|1-\lambda|}(c)$ has four preimages. Therefore, for $\lambda > 1$ and $\lambda < 0$, the map (1) becomes 4-to-1 or even ∞-to-1, and the analysis of this parameter regime lies beyond the scope of this paper.

2.2 The forward and backward critical sets

The point $J_0 := \{0\}$ is the *critical point* and the circle $J_1 := \partial\overline{\mathbb{D}}_{1-\lambda}(c)$, which divides the plane into regions with different numbers of preimages, is the *critical circle* of the map (1). At $\lambda = 1$ in (1), the circle J_1 has radius 0 and coincides with the critical value c of (2).

The forward and backward iterates of J_0 and J_1 play a special role in the organisation of the dynamics of (1) on the punctured complex plane. The preimages $J_{-k} := f^{-k}(J_0)$, $k \geq 0$, of J_0 consist of up to 2^k isolated points and their union forms the *backward critical set*

$$\mathcal{J}^- := \cup_{k\geq 0} J_{-k}.$$

Each point in the backward critical set $\mathcal{J}^-$ can be written according to its sequence of preimages, that is, $J_{-k}^{s_k\cdots s_1} := f_{s_k\cdots s_1}^{-k}(J_0)$ for some $(s_l)_{1\leq l\leq k} \in \{0,1\}^k$.

The images $J_k := f^{k-1}(J_1)$, $k \geq 1$, of J_1 are closed curves and their union forms the *forward critical set*

$$\mathcal{J}^+ := \cup_{k\geq 1} J_k.$$

In the nonchaotic parameter regime, the J_k are topological circles and we will refer them as circles throughout this paper. For $\lambda = 1$ in (1), the set $\mathcal{J}^+$ consists only of the orbit of c. We call the union of the backward and forward critical sets the *critical set* $\mathcal{J} := \mathcal{J}^- \cup \mathcal{J}^+$.

2.3 The stable and unstable sets

The dynamics of the map (1) on the plane is organised by the critical set $\mathcal{J}$, the Julia set and the stable and unstable sets of saddle fixed and periodic points. For a saddle fixed point p of the (1) and a neighbourhood V of p, we define the *local stable manifold* $W^s_{loc}(p)$ as

$$W^s_{\text{loc}}(p) := \{z \in \mathbb{C} : f^k(z) \in V \text{ for all } k \geq 0\}.$$

It is tangent to the stable eigenspace of p [Palis & de Melo(1982)]. The *stable set* $W^s(p)$ is defined as all preimages of $W^s_{loc}(p)$; that is,

$$W^s(p) := \bigcup_{k\geq 0} f^{-k}(W^s_{\text{loc}}(p)). \tag{6}$$

Due to the presence of multiple inverses for (1), the stable set consists of infinitely many disjoint branches and, thus, is not an immersed manifold [Mira *et al.*(1996)]; the branch that contains p is the *primary manifold* and we denote it $W^s_0(p)$. The infinitely many branches of $W^s(p)$ are connected by the points in points in the backward critical set $\mathcal{J}^-$, that is, $W^s(p)$ is not connected, but its closure $\overline{W^s(p)}$ is connected and given by

$$\overline{W^s(p)} = W^s(p) \cup \mathcal{J}^-.$$

We define the *local unstable manifold* $W^u_{\text{loc}}(p)$ of the neighbourhood V of p as the local stable manifold with respect to the local inverse f^{-1}_{loc} of f that satisfies $f^{-1}_{\text{loc}}(p) = p$, that is,

$$W^u_{\text{loc}}(p) := \{z \in \mathbb{C} : (f^{-1}_{\text{loc}})^k(z) \in V \text{ for all } k \geq 0\},$$

and it is tangent to the unstable eigenspace at p. The *unstable set* $W^u(p)$ is defined as all images of the local unstable manifold $W^u_{\text{loc}}(p)$; that is,

$$W^u(p) := \bigcup_{k\geq 0} f^k(W^u_{\text{loc}}(p)). \tag{7}$$

For a diffeomorphism, the set $W^u(p)$ is an immersed manifold, but for a noninvertible map, the images of $W^u_{\mathrm{loc}}(p)$ form a single continuous curve that may have self-intersections. Due to the rotational symmetry of the map (1), if for some $z \in \mathbb{C}\backslash\{0\}$ the two points z and $-z$ are both contained in $W^u(p)$, then $W^u(p)$ intersects itself at the point $f(z)$.

We define the stable and unstable sets of a k-periodic saddle point q as the union of the stable and unstable sets of its orbit under the kth iterate f^k of the map (1) [Palis & de Melo(1982)]; that is,

$$\begin{aligned} W^s(q) &:= \bigcup_{1\le l\le k} W^s_{f^k}(f^l(q)) \quad \text{and} \\ W^u(q) &:= \bigcup_{1\le l\le k} W^u_{f^k}(f^l(q)). \end{aligned}$$

We compute the unstable sets and the primary manifolds of the stable sets numerically with the method proposed in [Krauskopf & Osinga(1998)] and implemented in the DsTool environment [Back *et al.*(1992),England *et al.*(2004),Krauskopf & Osinga(2000)]; we then take successive preimages of the primary manifold to obtain an approximation of the stable set; see [Hittmeyer *et al.*(2013)] for more details.

2.4 Properties of the complex quadratic family

We now recall some basic facts of the complex quadratic family (2) as needed in our study; see, for example, [Blanchard(1984),Devaney(2003),Milnor(2006)] for more details and as an entry point to the literature. In particular, for all definitions and properties given here for the map (2), we refer to [Blanchard(1984)], unless specified otherwise. The origin is called the *critical point* and c is called the *critical value* of (2). Infinity is attracting for all $c \in \mathbb{C}$ and we denote its basin of attraction by $\mathcal{B}(\infty)$. For a fixed parameter value $c \in \mathbb{C}$ an important object in the phase space of (2) is the *Julia set*, which we denote $\mathcal{Y}$ and define as

$$\mathcal{Y} := \partial\mathcal{B}(\infty). \tag{8}$$

Alternatively, $\mathcal{Y}$ can be characterised as the closure of the repelling periodic points of (2). We remark that the Julia set is generally denoted J or $\mathcal{J}$ in the literature, which we use already for the critical set of (1); therefore, we use the symbol $\mathcal{Y}$, as motivated by the Russian version of the name Julia to denote the Julia set. The Julia set $\mathcal{Y}$ is nonempty and invariant under (2), as well as the two preimages of (2). Furthermore, $\mathcal{Y}$ is *perfect*, that is, every point in $\mathcal{Y}$ is accumulated by other points in $\mathcal{Y}$. If there is another attractor, then it must contain the critical value c in its basin of attraction, and $\mathcal{Y}$ also bounds this basin.

In fact, $\mathcal{Y}$ is either connected or totally disconnected, depending on the parameter $c \in \mathbb{C}$. More precisely, the Julia set $\mathcal{Y}$ and the orbit of the critical value c are related by a fundamental dichotomy: $\mathcal{Y}$ is connected if and only if the orbit of the critical value c is bounded, and $\mathcal{Y}$ is totally disconnected if and only if the orbit of c goes to infinity. If $\mathcal{Y}$ is connected, it bounds the open set $\mathcal{C} := \mathbb{C}\backslash(\mathcal{B}(\infty) \cup \mathcal{Y})$. For the complex quadratic family (2) this set is the interior of the so-called *filled Julia set* $\mathbb{C}\backslash\mathcal{B}(\infty)$ and the set of bounded components of the *Fatou set* $\mathbb{C}\backslash\mathcal{Y}$ [Carleson & Gamelin(1993)]. On the other hand, if $\mathcal{Y}$ is totally disconnected, then $\mathcal{C}$ is always empty. Note that $\mathcal{C}$ may also be empty if $\mathcal{Y}$ is connected.

The central object of study in the parameter space $\mathbb{C}$ is the *Mandelbrot set*, which encodes this dichotomy. It is denoted $\mathcal{M}$ and defined as

$$\mathcal{M} := \{c \in \mathbb{C} : \mathcal{Y} \text{ is connected}\}. \tag{9}$$

Alternatively, $\mathcal{M}$ can be characterised as

$$\mathcal{M} := \{c \in \mathbb{C} : f_1^k(c) \text{ stays bounded for } k \to \infty\}. \tag{10}$$

The Mandelbrot set $\mathcal{M}$ constitutes the bifurcation diagram of (2) in the c-plane that summarises the properties of the corresponding Julia sets. The set $\mathcal{M}$ itself is connected and the interior $\mathrm{int}(\mathcal{M})$ of $\mathcal{M}$ consists of cardioids and bulbs; see already Figure 1(b).

For c in a bulb or cardioid in $\mathrm{int}(\mathcal{M})$ the corresponding map (2) admits a unique (hyperbolic) attractor $\mathcal{P}_k = \{p_k^0, \ldots, p_k^{k-1}\}$ of some period k, which attracts the orbit of c. Let $\mathcal{B}(\mathcal{P}_k)$ denote the basin of attraction of $\mathcal{P}_k$. The *immediate basin of attraction* of $\mathcal{P}_k$, denoted $\mathcal{B}_0(\mathcal{P}_k)$, is the union of the k unique connected open subsets of $\mathcal{B}(\mathcal{P}_k)$ that contain p_k^l for $0 \leq l \leq k-1$. The basin $\mathcal{B}(\mathcal{P}_k)$ is the union of all preimages of $\mathcal{B}_0(\mathcal{P}_k)$ and forms the set $\mathcal{C}$. The Julia set $\mathcal{Y}$ is the boundary of $\mathcal{B}(\mathcal{P}_k)$ and consists of a union of Jordan curves. The Jordan curves that form $\mathcal{Y}$ typically contain no smooth arcs and are nowhere differentiable. Moreover, each bulb or cardioid of $\mathcal{M}$ contains one parameter value C_k in its interior, for which the critical value $c = \mathrm{C}_k \in \mathcal{P}_k$. This value is called the *centre* of the bulb or the cardioid and the corresponding attractor has zero as a double eigenvalue, that is, it is *super-attracting*.

For each c in the exterior $\mathrm{ext}(\mathcal{M})$ of $\mathcal{M}$, the orbit of c goes to infinity. In this case, the complex quadratic map (2) does not have any finite periodic attractors. Hence, the Julia set $\mathcal{Y}$ is no longer the boundary of a finite basin and the set $\mathcal{C}$ is empty. Instead, $\mathcal{Y}$ is totally disconnected and perfect, which means that it is a *Cantor set*.

For values $c \in \partial\mathcal{M}$, the Julia set $\mathcal{Y}$ is connected and the orbit of c stays bounded. If $c \in \partial M$ is pre-periodic, $\mathcal{Y}$ is a *dendrite*, that is, a locally connected, compact and connected set that does not contain any Jordan curves. However, the topology of Julia sets for $c \in \partial\mathcal{M}$ and the associated dynamics of (2) can be very different and much more complicated; see, for example, [Carleson & Gamelin(1993)].

Figure 1 shows the bifurcation diagram of the complex quadratic family (2). Panel (a) shows the attractors in the (c, z)-plane for $c, z \in \mathbb{R}$. The colours green, cyan, red and blue correspond to periodic windows, where (2) has attracting periodic orbits $\mathcal{P}_k$ of periods $k = 1$, 2, 3 and 4, respectively. We remark that, for c and z both real, (2) is topologically conjugate to the logistic map $x \mapsto \mu x(1-x)$ with $\mu, x \in \mathbb{R}$. The points S_1, P_1 and P_2 (black dots) are points of saddle-node and period-doubling bifurcations, respectively. When c is decreased along the real line, the restriction of (2) to $\mathbb{R}$ undergoes a sequence of period-doubling bifurcations, which leads to the appearance of a chaotic attractor in $\mathbb{R}$. Figure 1(b) shows the Mandelbrot set $\mathcal{M}$ in the complex c-plane. The main cardioid (green) corresponds to the existence of an attracting fixed point; the bulb containing C_2 (cyan) and the bulbs labelled 3 (red) and 4 (blue) correspond to the existence of attracting periodic points of periods two, three and four, respectively; the black bulbs correspond to attracting periodic points of higher periods. The points $\mathrm{C}_1 = 0$ and $\mathrm{C}_2 = -1$ (black dots) are the centres of the main cardioid and the period-two bulb, respectively, where the critical point J_0 is a super-attracting fixed point and period-two point, respectively. Indeed, panel (a) corresponds to the one-dimensional cross section along the line $\mathrm{Im}(c) = 0$ in panel (b).

2.5 Definition of the Julia set for $\lambda < 1$

Note that the bounded attractors of (1) may change drastically, but infinity is an attractor for all $\lambda \in (0, 1]$. Therefore, we define the Julia set of (1) for $\lambda \in (0, 1]$ by property (8), that is, as the boundary of the basin of attraction of infinity, and still denote it $\mathcal{Y}$. For $\lambda = 0$, infinity is no longer attracting. As we will see in Section 3.1, the basin $\mathcal{B}(\infty)$ goes to infinity as λ goes to 0 and, therefore, we define the Julia set to be $\mathcal{Y} := \{\infty\}$ for $\lambda = 0$.

We believe that this definition of the extension of the Julia set $\mathcal{Y}$ to the family of maps (1) is suitable, because our numerical investigations in Sections 3 and 4 indicate that $\mathcal{Y}$ retains its main properties. In particular, $\mathcal{Y}$ is invariant under (1) and both its preimages and it is nonempty. Moreover, our results suggest that $\mathcal{Y}$ is closed and perfect. However, as we will see in Section 4, for $\lambda \in (0, 1)$ the Julia set $\mathcal{Y}$, as defined by (8), is not necessarily the closure of the repelling periodic points. For some $\lambda \in (0, 1)$, a subset of $\mathcal{Y}$ lies in the interior of the disk bounded by the critical circle J_1. Since the points in this subset of $\mathcal{Y}$ have no preimage, they are not in the closure of the repelling periodic points. On the other hand, this subset eventually appears to map to the closure of the repelling periodic points. Therefore, we propose the alternative characterisation of the Julia set $\mathcal{Y}$ of map (1) for $\lambda \in [0, 1]$ as the closure of periodic and pre-periodic repelling points, that is, we conjecture that

$$\mathcal{Y} = \overline{\{z \in \mathbb{C} \ : \ \exists\, k \in \mathbb{N} \text{ such that } f^k(z) \text{ is a repelling periodic point}\}}.$$

In particular, this alternative characterisation of $\mathcal{Y}$ also holds for $\lambda = 1$, that is, for the complex quadratic family (2).

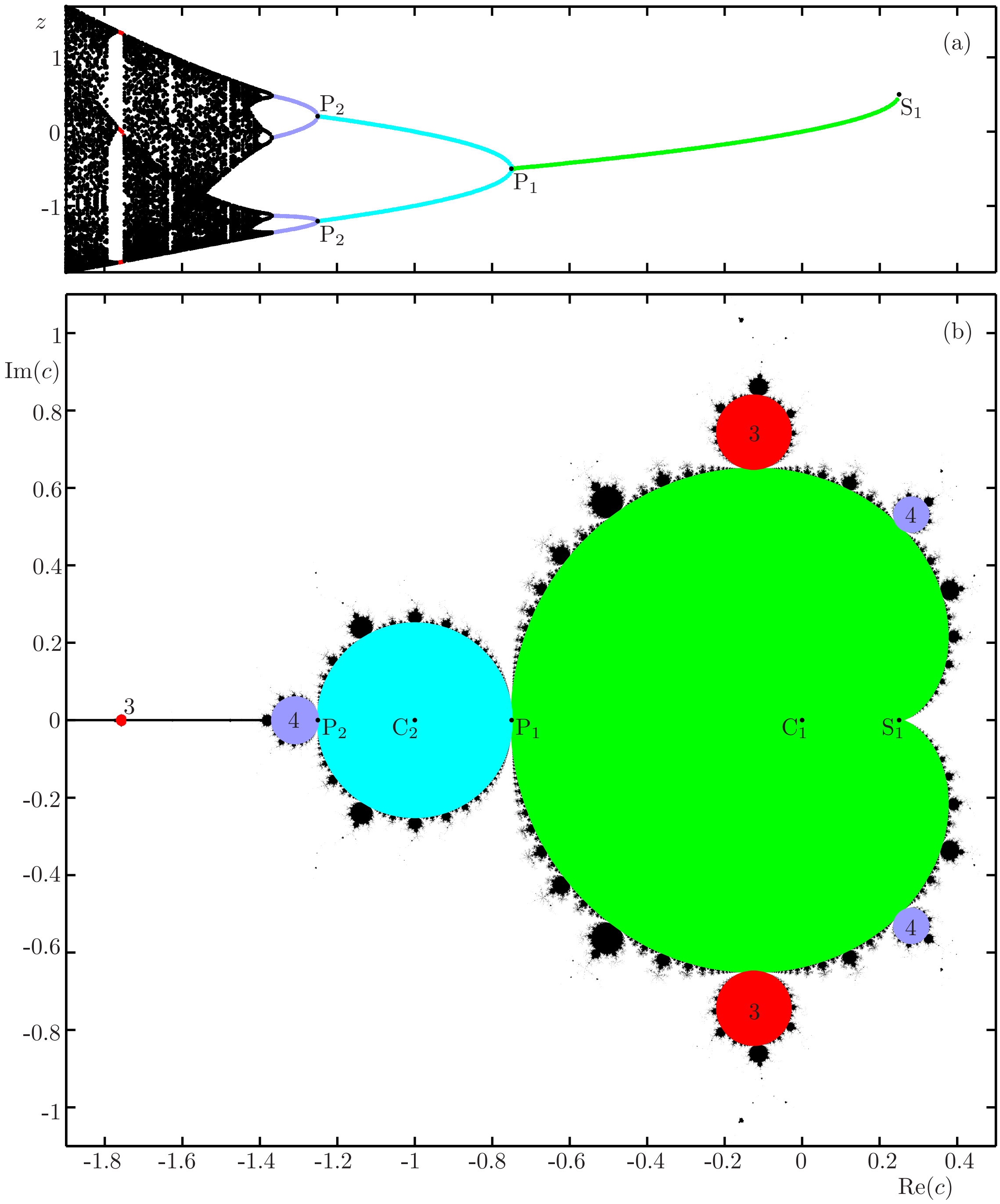

Figure 1: The bifurcation diagram of the map (2) in the (c, z)-plane for $c, z \in \mathbb{R}$ (a) and in the c-plane for $c, z \in \mathbb{C}$ (b). The colours green, cyan, red and blue correspond to the existence of attracting periodic points of periods one, two, three and four, respectively. The points S_1, P_1 and P_2 are points of saddle-node and period-doubling bifurcations, respectively, and the points C_1 and C_2 are the centres of the main cardioid and the period-two bulb, respectively.

2.6 Other perturbations of the complex quadratic family

The family (1) is a specific perturbation of the complex quadratic family (2); it is nonanalytic and has a singularity at $J_0 = 0$ for $\lambda \neq 1$. Moreover, (1) remains in the class of quadratic maps and admits infinitely many critical orbits, namely, the orbits of all points on the critical circle J_1. Other perturbations of the complex quadratic family (2) have been studied, for example, in [Bielefeld *et al.*(1993), Devaney(2013), Bruin & van Noort(2004), Blanchard *et al.*(2005), Marotta(2008), McMullen(1988), Peckham(1998), Peckham & Montaldi(2000)]. In [Blanchard *et al.*(2005), Devaney(2013), Marotta(2008), McMullen(1988)] the map (2) is perturbed to a rational map with a pole at $J_0 = 0$ by adding the term α/z^m for $m \in \mathbb{N}$ with $m \geq 1$. For $\alpha \neq 0$, the perturbed maps are rational maps of degree $2 + m$ and analytic on $\mathbb{C}\backslash\{0\}$. For $m = 1$, $m = 2$ and $m \geq 3$ and certain $\alpha, c \in \mathbb{C}$ the Julia set of the perturbed map is homeomorphic to a so-called *Sierpinski gasket*, a *Sierpinski carpet* or a *Cantor set of circles*, respectively. The Sierpinski gasket is constructed by dividing a triangular region of the plane into four equal-sized subtriangles, removing the open middle triangle and repeating this step with the remaining triangles infinitely many times. Similarly, the Sierpinski carpet is constructed by dividing a square into nine equal-sized subsquares, removing the open middle square and repeating this step with the remaining squares infinitely many times. A Cantor set of circles is a union of infinitely many nested Jordan curves such that their intersection with a line is a Cantor set.

In [Bielefeld *et al.*(1993), Bruin & van Noort(2004)] the map $z \mapsto |z|^{2\alpha-2}z^2 + c$ is considered near $\alpha = 1$, which is, in fact, map (3) for $\lambda = 1$ and $a = 2\alpha$; the perturbed map is nonanalytic, is no longer quadratic and has a singularity at $J_0 = 0$. In [Peckham(1998), Peckham & Montaldi(2000)] the map (2) is perturbed to a nonanalytic map by adding the term $A\bar{z}$ with $A \in \mathbb{C}$ near $A = 0$. In [Bielefeld *et al.*(1993), Bruin & van Noort(2004), Peckham(1998), Peckham & Montaldi(2000)] the bifurcation diagram of the perturbed maps is studied in the c-plane, that is, the analogue of the Mandelbrot set $\mathcal{M}$, for different $\alpha \in \mathbb{R}$ near $\alpha = 1$ and $A \in \mathbb{C}$ near $A = 0$, respectively. They find saddle-node, period-doubling and Neimarck–Sacker bifurcation curves, which give rise to resonance tongues and invariant circles near the cusp point C_1, the period-doubling point P_1 and the point between the main cardioid and the period-three bulb of the unperturbed map. In [McDonald *et al.*(1985a), McDonald *et al.*(1985b)] nonanalytic quadratic maps of the plane are considered, where chaotic attractors interact with their fractal basin boundaries; however, they consider a parameter regime far away from (2). All of these perturbations of the complex quadratic map have in common that they admit only one critical orbit and are either nonanalytic or have a singularity at J_0.

3 The parameter c in the main cardioid of the Mandelbrot set $\mathcal{M}$

In this section we consider three different fixed values of c in the interior of the main cardioid of the Mandelbrot set $\mathcal{M}$. We first consider the special case $c = 0$ in Section 3.1, because for $\lambda = 1$ the origin of (2) is super-attracting and the Julia set $\mathcal{Y}$ is simply the unit circle. In the sections that follow, we choose $c = 0.1 > 0$ and $c = -0.25 < 0$, so that (1) is orientation preserving and orientation reversing, respectively. For all choices of c, we start from $\lambda = 1$ and investigate the changes in the phase portrait of map (1) for decreasing $\lambda \in [0, 1]$.

3.1 The special case $c = 0$

First, we consider the special case $c = 0$, which is the centre of the main cardioid of $\mathcal{M}$, meaning that $c = f(c) = 0$ is a super-attracting fixed point of (2).

Figure 2(a) is the phase portrait of (1) for $c = 0$ and $\lambda = 1$, that is, of the complex quadratic map (2), which is defined for all $z \in \mathbb{C}$. The critical point $J_0 = 0$ (green dot) is mapped to the critical value $J_1 = 0$ (green dot) of (2). Therefore, J_0 is equal to the fixed point p_1 (blue triangle), which is super-attracting. The points inside the unit circle form the basin of attraction $\mathcal{B}(p_1)$ (white) and $\mathcal{B}(\infty)$ (grey) consists of all points outside the unit circle. The grey scale corresponds to sets with different escape times to a neighbourhood of infinity, chosen to be the set of points $\{z \in \mathbb{C} \ : \ |z| > 2r\}$, where r is the maximum value of $\mathrm{Re}(z)$ shown in the phase portrait. The unit circle forms the boundary between $\mathcal{B}(p_1)$ and $\mathcal{B}(\infty)$ and, hence, is the Julia set $\mathcal{Y}$ (black). Restricted to $\mathcal{Y}$, the map (1) with $(c, \lambda) = (0, 1)$ is the angle-doubling map $\theta \mapsto 2\theta \pmod 1$. Therefore, (1) is chaotic on $\mathcal{Y}$ and repelling periodic points are dense in it [Devaney(2003)]. We show only fixed points and period-two points in Figure 2(a). The map has a repelling fixed point $s_1 = 1 \in \mathcal{Y}$ (red square) on the real line and two repelling period-two points $s_2^{\pm} = \pm\exp(2\pi i/3) \in \mathcal{Y}$ (red squares) above and below the real line, respectively. Since p_1 and infinity are the only attractors, the set $\mathcal{C} = \mathbb{C}\backslash(\mathcal{B}(\infty) \cup \mathcal{Y})$ is simply the basin $\mathcal{B}(p_1)$.

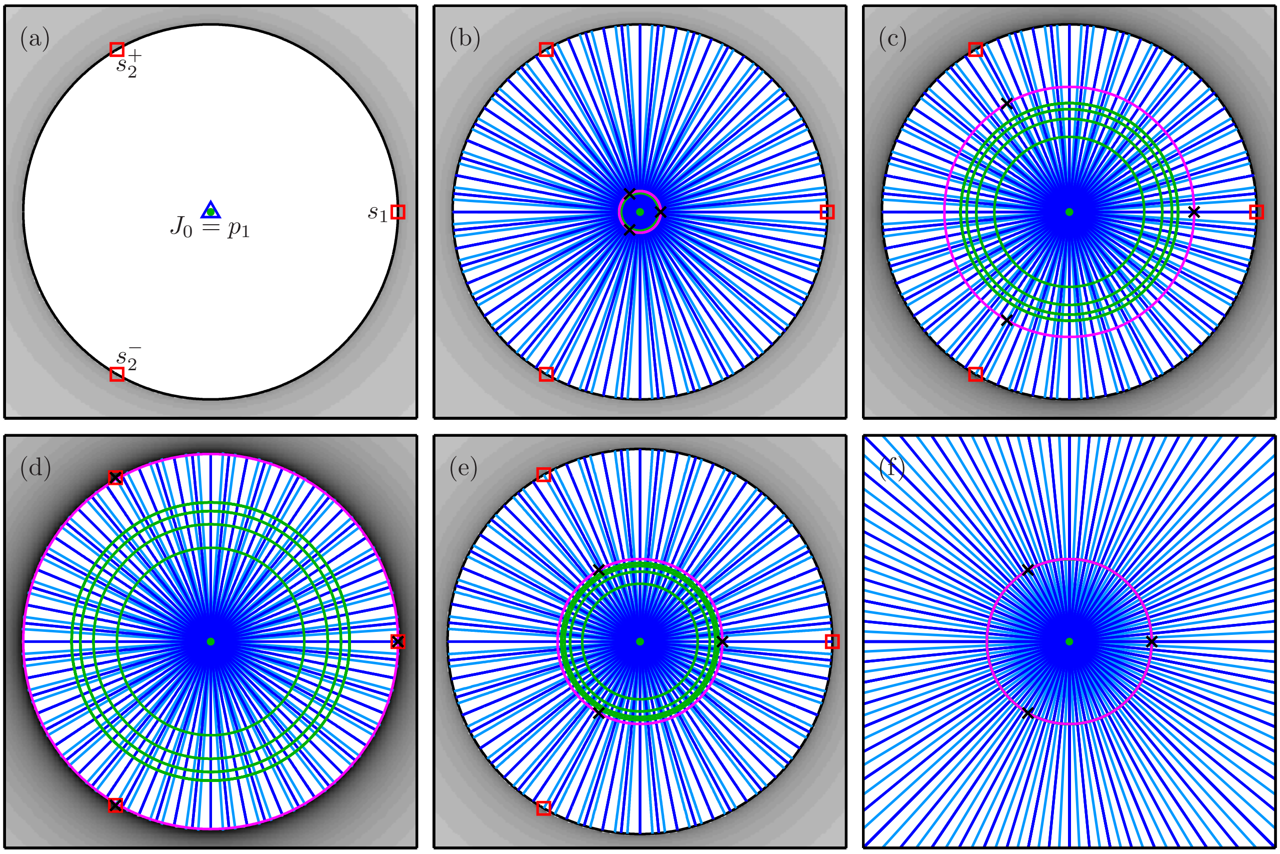

Figure 2: The transition of the phase portrait for $c = 0$ in $[-1.1, 1.1] \times [-1.1, 1.1]$ in panels (a)–(d) and $[-2.5, 2.5] \times [-2.5, 2.5]$ in panels (e) and (f), respectively; shown are the Julia set $\mathcal{Y}$ (black), the critical set $\mathcal{J}$ (green), the fixed points p_1 (blue triangle/black cross) and s_1 (red square), the period-two points $p_2^{\pm}$ (black crosses) and $s_2^{\pm}$ (red squares), the stable sets $W^s(p_1)$ (dark blue) and $W^s(p_2^{\pm})$ (light blue), respectively, and the chaotic attractor $\mathcal{A}$ (magenta). Panels (a)–(f) are for $\lambda = 1$, $\lambda = 0.9$, $\lambda = 0.6$, $\lambda = 0.5$, $\lambda = 0.3$ and $\lambda = 0$, respectively.

Figures 2(b) and (c) are the phase portraits for $\lambda = 0.9$ and $\lambda = 0.6$, respectively. As λ is decreased from $\lambda = 1$, the critical value $J_1 = 0$ opens up to the critical circle J_1 (green) with radius $1 - \lambda$ around 0. The Julia set $\mathcal{Y}$ is still the unit circle and contains the repelling points s_1 and $s_2^{\pm}$ along with other repelling periodic points. However, the period-one attractor p_1 is now a saddle point (black cross) on the positive real line and the map has two period-two saddle points p_2^+ and p_2^- above and below the real line, respectively. All saddles lie on a circle with radius $(1-\lambda)/\lambda$ around J_0 (magenta), which we call $\mathcal{A}$. The images of J_1 in the forward critical set $\mathcal{J}^+$ are concentric circles that accumulate on $\mathcal{A}$. One can show that the circle $\mathcal{A}$ is invariant under (1), that it attracts all points inside $\mathcal{Y}$, and that the restriction of (1) to $\mathcal{A}$ is the angle-doubling map. Therefore, $\mathcal{A}$ is a chaotic attractor and saddle periodic points of (1) are dense in it. Its basin $\mathcal{B}(\mathcal{A})$ (white) is bounded by $\mathcal{Y}$. In other words, for the special case $c = 0$ we obtain a chaotic attractor, namely, the circle of radius $(1-\lambda)/\lambda$ around J_0, for any $\lambda \in (0.5, 1)$. The saddle points p_1 and $p_2^{\pm}$ have one-dimensional stable sets, denoted $W^s(p_1)$ (dark blue) and $W^s(p_2^{\pm})$ (light blue), respectively. The primary branches $W_0^s(p_1)$ and $W_0^s(p_2^{\pm})$ are arcs that go through p_1 and $p_2^{\pm}$ and connect to J_0 on one side and to s_1 and $s_2^{\pm}$ on the other, respectively. The sets $W^s(p_1)$ and $W^s(p_2^{\pm})$ consist of infinitely many straight lines, which go through the preimages of p_1 and $p_2^{\pm}$ on $\mathcal{A}$ and extend to J_0 on one side and to the preimages of s_1 and $s_2^{\pm}$ on $\mathcal{Y}$ on the other, respectively. These infinitely many branches all connect up at J_0, but they have no other branch points, because J_0 lies inside J_1.

As λ decreases further, the radius of $\mathcal{A}$ increases until, for $\lambda = 0.5$, it equals 1 and $\mathcal{A}$ and $\mathcal{Y}$ coincide. Figure 2(d) is the phase portrait for $\lambda = 0.5$. We observe that the fixed points p_1 and s_1 and the period-two points $p_2^{\pm}$ and $s_2^{\pm}$ meet in a transcritical bifurcation; they have one eigenvalue equal to 1. This bifurcation is highly degenerate, because all saddle periodic points in $\mathcal{A}$ have transcritical bifurcations with corresponding repelling periodic points in $\mathcal{Y}$ at the same time. Note that $\mathcal{A}$ still attracts all points bounded by $\mathcal{Y}$, including the circles in $\mathcal{J}^+$, but the attraction is no longer exponential. In particular, $\mathcal{A}$ is not an attractor, because we cannot find a neighbourhood, in which all points converge to $\mathcal{A}$.

Past the degenerate transcritical bifurcation, $\mathcal{A}$ and $\mathcal{Y}$ move apart again. However, now the chaotic attractor $\mathcal{A}$ is the unit circle and $\mathcal{Y}$ is the circle with radius $(1-\lambda)/\lambda$ around 0. (Note that the radius of $\mathcal{Y}$ must be equal or larger than the radius of $\mathcal{A}$, because infinity is attracting for all $\lambda \in (0, 1]$.) Figure 2(e) is the phase portrait for $\lambda = 0.3$. The dynamics of map (1) for $\lambda \in (0, 0.5)$ are qualitatively the same as the dynamics for $\lambda \in (0.5, 1)$, that is, $\mathcal{A}$ and $\mathcal{Y}$ are circles around J_0 and the stable sets $W^s(p_1)$ and $W^s(p_2^{\pm})$ are formed by infinitely many straight lines between J_0 and the preimages of s_1 and $s_2^{\pm}$ on $\mathcal{Y}$, respectively. Note that the range shown in Figure 2 varies from $[-1.1, 1.1] \times [-1.1, 1.1]$ in panels (a)–(d) to $[-2.5, 2.5] \times [-2.5, 2.5]$ in panel (e) due to the increased radius of $\mathcal{Y}$.

Finally, as $\lambda \to 0$, the radius $1-\lambda$ of J_1 goes to 1 and the radius $(1-\lambda)/\lambda$ of $\mathcal{Y}$ goes to infinity, while $\mathcal{A}$ remains the unit circle. The phase portrait for $\lambda = 0$ is shown in Figure 2(f), where map (1) reduces to $z \mapsto (z/|z|)^2$, which is (5) for $c = 0$; the range shown is the same as in panel (e). The forward critical set $\mathcal{J}^+$ consists only of the critical circle J_1, which coincides with the chaotic attractor $\mathcal{A}$. Its basin $\mathcal{B}(\mathcal{A})$ is the entire punctured plane, which is mapped onto $\mathcal{A}$ in an ∞-to-1 fashion. Note that the stable sets $W^s(p_1)$ and $W^s(p_2^{\pm})$ are still defined as in equation (6) in Section 2.3. More specifically, $W^s(p_1)$ and $W^s(p_2^{\pm})$ are straight lines from J_0 through the preimages of p_1 and $p_2^{\pm}$ in $\mathcal{A}$; each such line extends to infinity and each point on it immediately maps to p_1 or $p_2^{\pm}$, respectively.

3.2 Global transitions for $c = 0.1$

We now consider an orientation-preserving case in $\mathcal{M}$; namely, we choose $c = 0.1$ to the right of the centre $c = 0$ of the main cardioid of $\mathcal{M}$. As before, we study the changes in the phase portrait of map (1) when $\lambda \in [0, 1]$ is decreased from $\lambda = 1$; the corresponding phase portrait is shown in Figure 3(a). As $c = 0.1$ lies in the interior of the main cardioid of $\mathcal{M}$, the map has a fixed-point attractor on the real line, denoted p_1 (blue triangle); the Julia set $\mathcal{Y}$ (black) is a Jordan curve and coincides with the closure of the repelling periodic points. We computed $\mathcal{Y}$ by plotting up to the third preimage of approximately three thousand repelling periodic points with periods up to 24. The map has a repelling fixed point (red square), denoted s_1, which lies on the intersection of $\mathcal{Y}$ with the real line. The basin $\mathcal{B}(p_1)$ (white) of the attractor p_1 is the set $\mathcal{C} = \mathbb{C}\backslash(\mathcal{B}(\infty) \cup \mathcal{Y})$. The basin $\mathcal{B}(\infty)$ is show in grey. The backward critical set $\mathcal{J}^-$ (green dots) is shown up to the sixth preimage J_{-6} of the critical point J_0; it accumulates on the Julia set $\mathcal{Y}$. The forward critical set $\mathcal{J}^+$ (green dots) is shown up to the fifth image J_6 of the critical value $J_1 = 0.1$ (green dot) of (2); it converges to p_1.

As soon as $\lambda < 1$, the critical circle J_1 becomes a proper circle with radius $1-\lambda$; note that this circle is now centred at $c = 0.1$. Figure 3(b) shows the phase portrait for $\lambda = 0.95$. The critical circle J_1 has radius $1-\lambda = 0.05$ and the forward critical set $\mathcal{J}^+$ consists of closed curves accordingly. The map (1) is no longer analytic, but the dynamics of the key objects are qualitatively the same as for $\lambda = 1$ in panel (a): the attractor p_1 and the repellor s_1 are the only fixed points, the circles in the forward critical set $\mathcal{J}^+$ accumulate on p_1, the backward critical set $\mathcal{J}^-$ accumulates on $\mathcal{Y}$, which is a Jordan curve bounding $\mathcal{C} = \mathcal{B}(p_1)$. Since the orbits of all points on J_1 are attracted by p_1, one could still think of J_1 as the image of J_0 and so the entire critical set $\mathcal{J}$ lies in $\mathcal{C} = \mathcal{B}(p_1)$. Here, $\mathcal{Y}$ can still be viewed as the closure of the repelling periodic points.

As λ decreases, p_1 destabilises in a pitchfork bifurcation at $\lambda \approx 0.9375$. The fixed point p_1 becomes a saddle and two attracting fixed points $q_1^{\pm}$ are born, which are each others symmetric counterparts under complex conjugation. Figures 3(c) for $\lambda = 0.93$ and (d) for $\lambda = 0.91$ show two phase portraits after the pitchfork bifurcation. The saddle p_1 (black cross) has one-dimensional stable and unstable sets $W^s(p_1)$ (blue) and $W^u(p_1)$ (red), respectively. The primary branch $W_0^s(p_1)$ of $W^s(p_1)$ is the open interval (J_0, s_1) on the real line. The stable set $W^s(p_1)$ consists of infinitely many branches, formed by the preimages of $W_0^s(p_1)$, which contain the preimages of p_1 and end at the preimages of s_1 in $\mathcal{Y}$. In contrast to the case $c = 0$, where all branches of

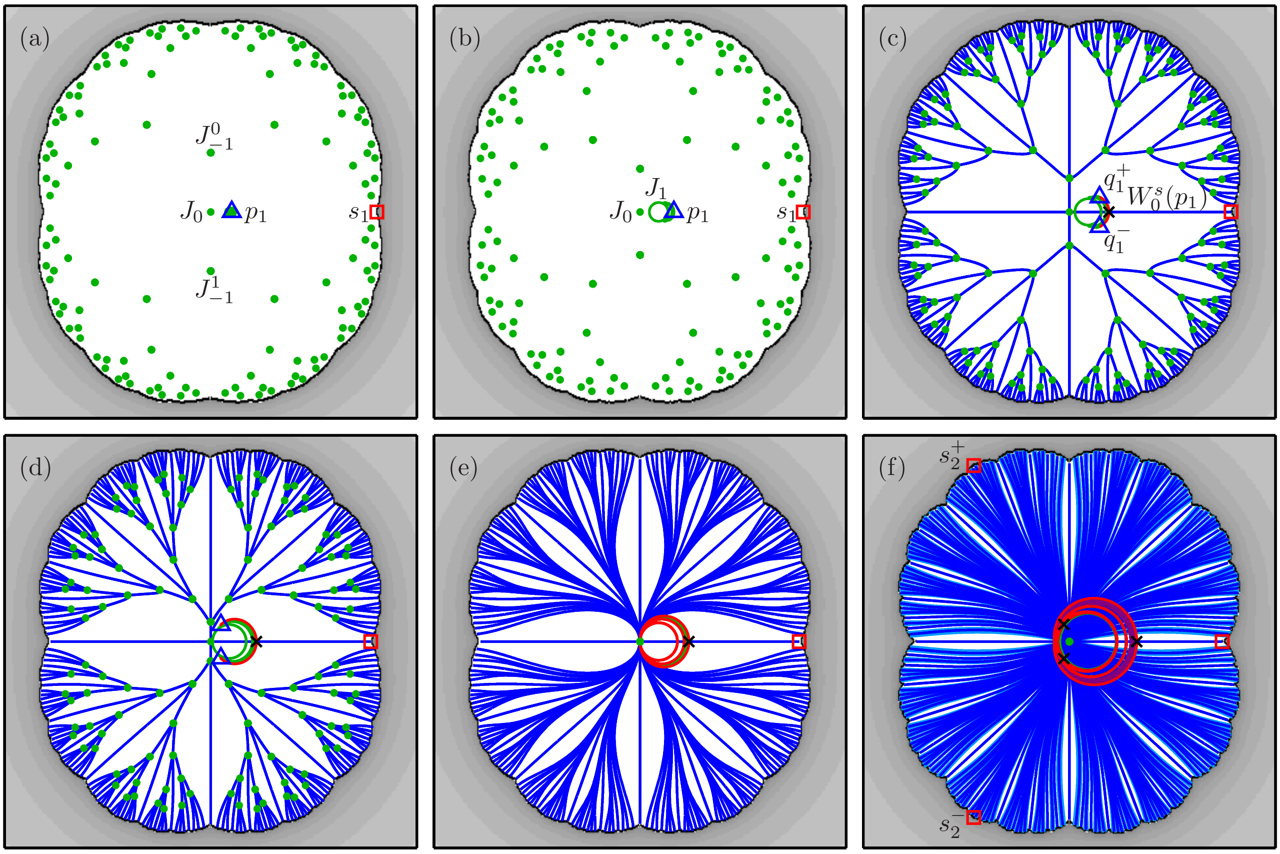

Figure 3: First step in the transition of the phase portrait for $c = 0.1$ in $[-1.1, 1.1] \times [-1.1, 1.1]$; shown are the Julia set $\mathcal{Y}$ (black), the critical set $\mathcal{J}$ (green), the fixed points p_1 (blue triangle/black cross), s_1 (red square) and $q_1^{\pm}$ (blue triangles), the period-two points $p_2^{\pm}$ (black crosses) and $s_2^{\pm}$ (red squares), and their stable and unstable sets, denoted $W^s(p_1)$ (dark blue), $W^s(p_2^{\pm})$ (light blue), $W^u(p_1)$ (red), and $W^u(p_2)$ (purple), respectively. Panels (a)–(f) are for $\lambda = 1$, $\lambda = 0.95$, $\lambda = 0.93$, $\lambda = 0.91$, $\lambda = 0.9$, and $\lambda = 0.85$, respectively.

$W^s(p_1)$ emanate from J_0, $W^s(p_1)$ now has a tree structure: the branches of $W^s(p_1)$ are connected at points in $\mathcal{J}^-$ such that each point in $\mathcal{J}^-$ connects four branches of $W^s(p_1)$. The unstable set $W^u(p_1)$ lies outside the critical circle J_1; its two sides are curves that end at $q_1^{\pm}$. The circles in the forward critical set $\mathcal{J}^+$ accumulate on the closure of $W^u(p_1)$, that is, on $W^u(p_1) \cup \{q_1^{\pm}\}$. Note, however, that individual orbits of points on J_1 converge to either p_1, q_1^+ or q_1^-. More precisely, the two points in $J_1 \cap \mathbb{R}$ lie in $W^s(p_1)$, but all other points on J_1 lie in one of the basins of $q_1^{\pm}$, denoted $\mathcal{B}(q_1^{\pm})$. The Julia set $\mathcal{Y}$ is still a Jordan curve, but the set $\mathcal{C}$ is no longer the basin of a single attractor. Instead, $\mathcal{C}$ now consists of the two basins $\mathcal{B}(q_1^{\pm})$, as well as the backward critical set $\mathcal{J}^-$ and the stable set $W^s(p_1)$, which form the boundary between the two basins $\mathcal{B}(q_1^{\pm})$.

As λ decreases further, map (1) undergoes a first homoclinic tangency of the stable and unstable sets $W^s(p_1)$ and $W^u(p_1)$ at $\lambda \approx 0.900085$ and a first backward critical tangency of the backward critical set $\mathcal{J}^-$ and $W^u(p_1)$ at $\lambda \approx 0.90006$. At a backward critical tangency $W^u(p_1)$ contains J_0 and a sequence of its preimages in $\mathcal{J}^-$; after such a tangency $W^u(p_1)$ forms self-intersecting loops around the circles in $\mathcal{J}^+$. The first homoclinic tangency is accumulated by an infinite sequence of homoclinic tangencies and an infinite sequence of forward critical tangencies, that is, tangencies between $\mathcal{J}^+$ and $W^s(p_1)$. Similarly, the first backward critical tangency is accumulated by an infinite sequence of backward critical tangencies and an infinite sequence of forward-backward critical tangencies, that is, tangencies between $\mathcal{J}^+$ and $\mathcal{J}^-$; see [Hittmeyer *et al.*(2013)] for more details.

Figure 3(e) is the phase portrait for $\lambda = 0.9$, where J_1 has radius $1 - \lambda = 0.1$, such that the critical point J_0 lies on the critical circle J_1 in a forward-backward critical tangency. This bifurcation is the "last" forward-backward critical tangency. All points in $\mathcal{J}^-$ have disappeared into J_0 and J_0 no longer has any preimages. Accordingly, the infinitely many branches of $W^s(p_1)$ now all connect at J_0, which means that the tree structure of $W^s(p_1)$ has collapsed into J_0. Similar to the case $c = 0$, the stable set $W^s(p_1)$ consists of infinitely many arcs extending to J_0 at one end and to the preimages of p_1 in $\mathcal{Y}$ at the other; compare with Figure 2. Since $J_0 \in J_1$, the circle J_2 contains J_1 and, similarly, we have $J_l \subset J_k$ for all $1 \leq l \leq k$. The attractors $q_1^{\pm}$ have disappeared into J_0 and the unstable set $W^u(p_1)$ intersects itself in several points on the real line. Let $W_0^u(p_1)$ be the closed segment of $W^u(p_1)$ containing p_1 up to the first intersection point of the two sides of $W^u(p_1)$. Then the circles in $\mathcal{J}^+$ and the entire unstable set $W^u(p_1)$ are bounded by $W_0^u(p_1)$. As we will show in Figure 4, our numerical calculations suggest that the closure of $W^u(p_1)$ is now a chaotic attractor $\mathcal{A}$ and saddle periodic points are dense in it. In Figure 3(e), the set $\mathcal{C}$ is the basin of attraction $\mathcal{B}(\mathcal{A})$ of $\mathcal{A}$. In particular, since p_1 is contained in $\mathcal{A}$, its stable set $W^s(p_1)$ is contained in the basin $\mathcal{B}(\mathcal{A})$.

Figure 3(f) is the phase portrait for $\lambda = 0.85$, after the forward-backward critical tangency of J_0 and J_1. Note that J_0 now lies inside the disk bounded by J_1. Two saddle period-two points (black crosses), denoted $p_2^{\pm}$, which are symmetric under complex conjugation, have appeared near J_0, but outside J_1. They have one-dimensional stable and unstable sets $W^s(p_2^{\pm})$ (light blue) and $W^u(p_2)$ (purple), respectively. The stable set $W^s(p_2^{\pm})$ consists of infinitely many branches connecting J_0 to the preimages of two period-two repelling points $s_2^{\pm}$ in $\mathcal{Y}$. The unstable set $W^u(p_2)$ accumulates on the chaotic attractor $\mathcal{A}$. Overall, the dynamics are somewhat similar to that of the special case $c = 0$ with $\lambda \in (0, 0.5) \cup (0.5, 1)$ in Figure 2, but, the chaotic attractor $\mathcal{A}$ and the Julia set $\mathcal{Y}$ are not circles.

Details of the last forward-backward critical tangency

We now look closer at how the critical set $\mathcal{J}$ changes and how fixed and periodic points appear or disappear in the forward-backward critical tangency of the critical point J_0 and the critical circle J_1 at $\lambda = 0.9$; see panels (e) and (f) of Figure 3. Figure 4 shows images before the bifurcation in column (a), at the bifurcation in column (b) and after the bifurcation in column (c), namely for $\lambda = 0.904$, $\lambda = 0.9$ and $\lambda = 0.89$, respectively. The top row shows J_0 and its preimages J_{-1}^1, J_{-2}^{00}, J_{-2}^{01}, J_{-2}^{10}, $J_{-2}^{20} \in \mathcal{J}^-$ (green points), and J_1 and its image $J_2 \in \mathcal{J}^+$ (green curves); the middle row shows enlargements near J_0, $q_1^{\pm}$ and $p_2^{\pm}$; and the bottom row shows, in addition, the saddle point p_1, its unstable set $W^u(p_1)$ and all saddle periodic points up to period 20.

Figure 4(a) illustrates the situation before the forward backward critical tangency; here, the point J_0 lies outside the disk bounded by J_1 and, accordingly, J_1 lies outside the region bounded by J_2. From (1) it is not hard to find that the attractors $q_1^{\pm}$ lie in the intersection of two circles, one around c with radius c and the other around 0 with radius $\sqrt{(c - 1 + \lambda)/\lambda}$. Therefore, $q_1^{\pm}$ lie outside the critical circle J_1 and its images. The points $q_1^{\pm}$ are the only attractors and the point p_1 is the only saddle.

At $\lambda = 0.9$, at the moment of bifurcation, J_0 lies on J_1, as shown in panels (b1) and (b2). Therefore, $J_1 \subset J_2$ and the preimages J_{-1}^0, J_{-1}^1, J_{-2}^{00}, J_{-2}^{01}, J_{-2}^{10}, J_{-2}^{20} of J_0 disappear. Furthermore, the circle around J_0 with radius $\sqrt{(c - 1 + \lambda)/\lambda}$ shrinks to the point J_0 and, thus, $q_1^{\pm}$ also disappear into J_0. Since $W^u(p)$ extends to $q_1^{\pm}$, the critical point J_0 now lies on the unstable set $W^u(p_1)$ in a last backward critical tangency, as shown in panel (b3). This backward critical tangency is degenerate because it coincides with the last forward critical tangency and, as a consequence, $W^u(p_1)$ does not form cusps at the circles in $\mathcal{J}^+$. This panel also shows saddle periodic points with periods $3 \leq k \leq 20$, but the saddle periodic points with periods $3 \leq k \leq 8$ are very close to J_0. There is an infinite sequence of forward-backward critical tangencies between the first backward critical tangency at $\lambda \approx 0.90006$ and the last forward-backward critical tangency at $\lambda = 0.9$; see [Hittmeyer *et al.*(2013)] for more details. We believe that each of these forward-backward critical tangencies gives rise to a saddle periodic orbit near J_0 and, as a result, (1) admits infinitely many saddle periodic points of arbitrarily high periods at $\lambda = 0.9$. Since these saddle periodic points accumulate on $W^u(p_1)$, and $W^u(p_1)$ is bounded, the closure of $W^u(p_1)$ is a chaotic attractor $\mathcal{A}$.

After the bifurcation, J_0 lies in the interior of the disk bounded by J_1; see panels (c1) and (c2). Because of the angle doubling of (1), the closed curve J_2 goes around J_1 twice and intersects itself on the negative real line. This means that the curves in the forward critical set $\mathcal{J}^+$ lie nested. Two period-two saddle points $p_2^{\pm}$

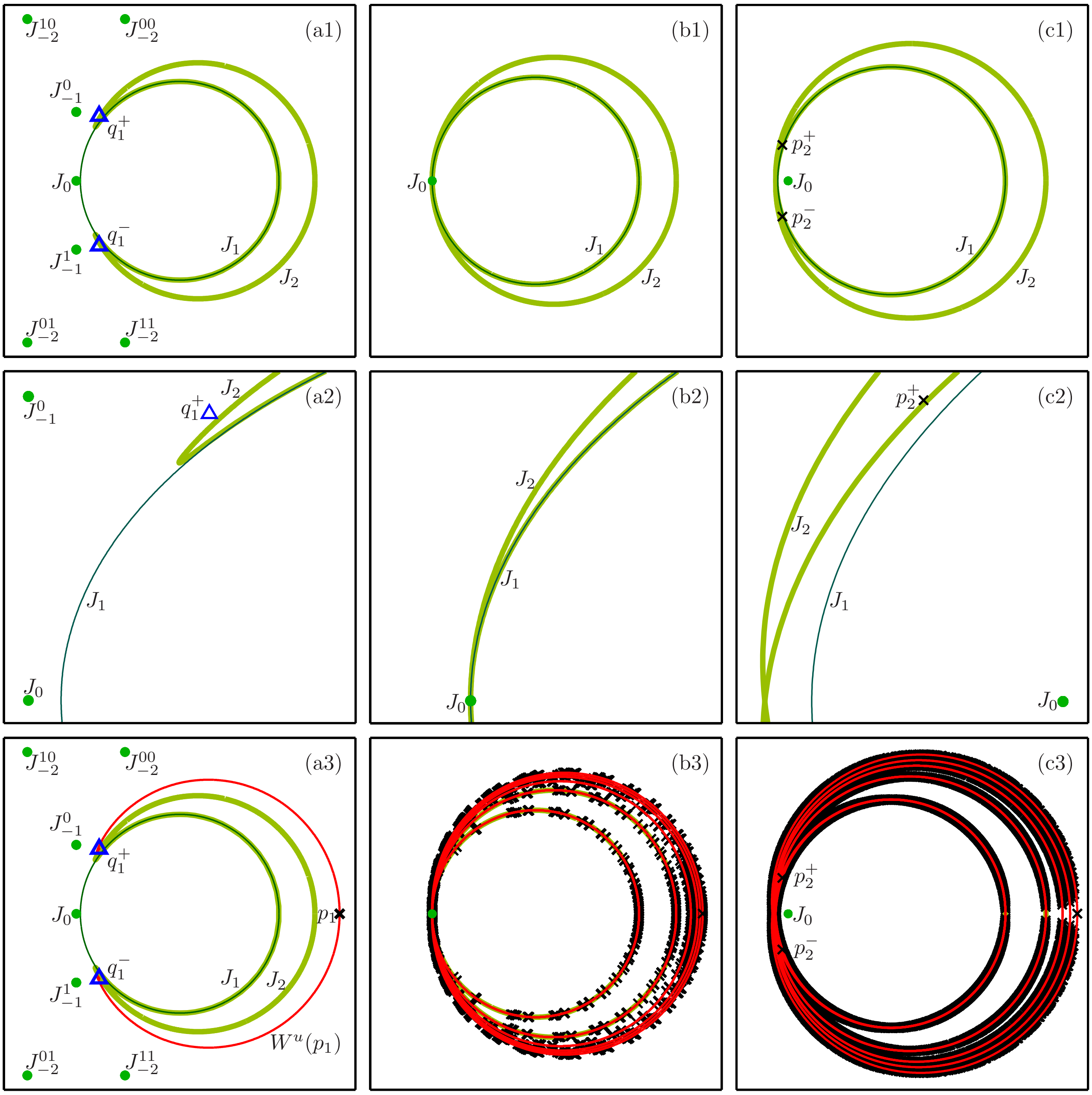

Figure 4: The effect of the "last" forward-backward critical tangency at $\lambda = 0.9$; row one and two show J_0 and its preimages J^0_{-1}, J^1_{-1}, J^{00}_{-2}, J^{01}_{-2}, J^{10}_{-2}, $J^{11}_{-2} \in \mathcal{J}^-$ (green), J_1 (dark green) and its image $J_2 \in \mathcal{J}^+$ (green), the attracting fixed points $q_1^{\pm}$ (blue triangles) and the period-two points $p_2^{\pm}$ (black crosses); row three shows, in addition, the saddle point p_1 (black cross), its unstable set $W^u(p_1)$ (red) and all saddle periodic points up to period 20. The parameter values are $\lambda = 0.904$ before the tangency in column (a), $\lambda = 0.9$ at the tangency in column (b) and $\lambda = 0.89$ after the tangency in column (c).

have appeared near J_0, which lie between the outer and the inner closed curve of J_2; see panel (c2). The saddle points $p_2^{\pm}$ were created in the last forward-backward critical tangency with the same mechanism by which the infinitely many saddles with periods $k \geq 3$ were created in the preceding infinite sequence of forward-backward

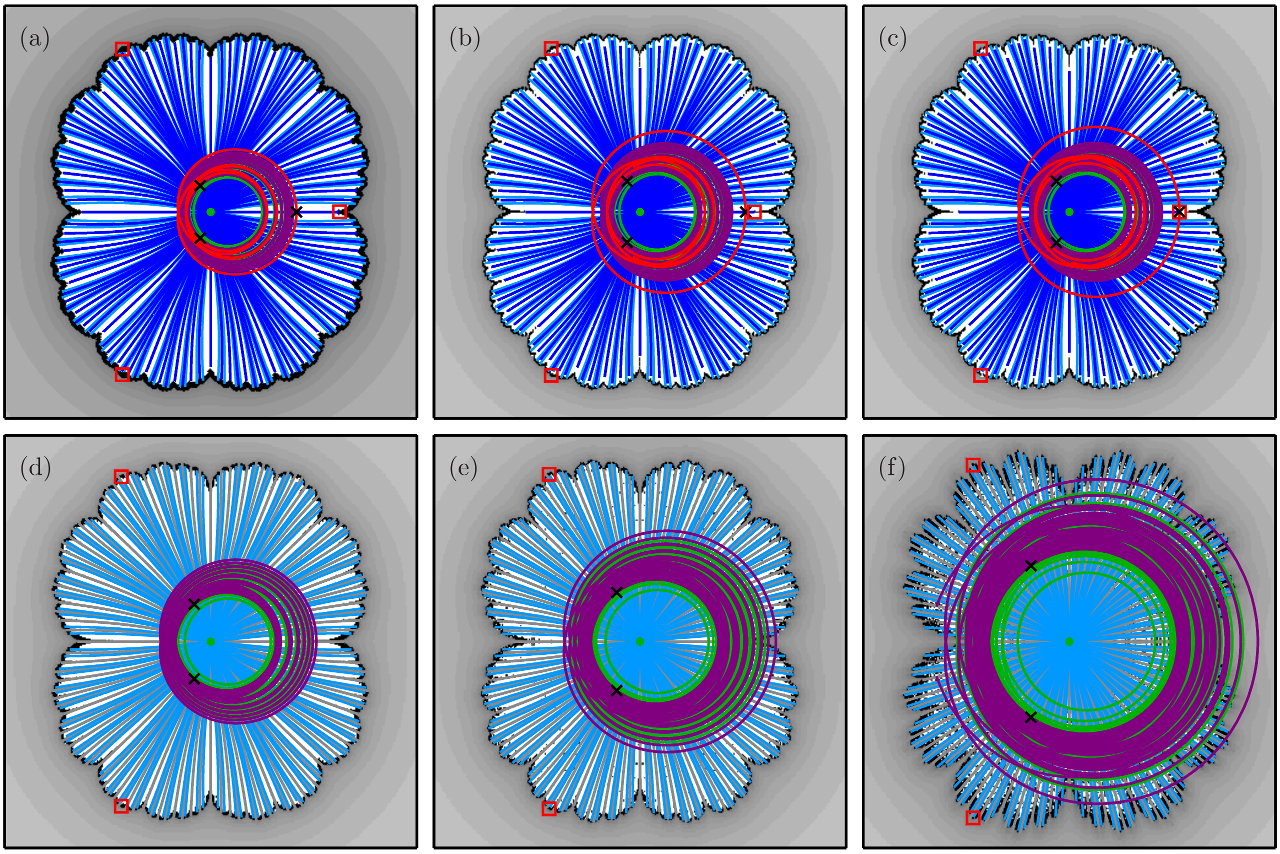

Figure 5: Second step in the transition of the phase portrait for $c = 0.1$ in $[-1.2, 1.2] \times [-1.2, 1.2]$; shown are the Julia set $\mathcal{Y}$ (black), the critical set $\mathcal{J}$ (green), the fixed points p_1 (black cross) and s_1 (red square), the period-two points $p_2^{\pm}$ (black crosses) and $s_2^{\pm}$ (red squares), and their stable and unstable sets $W^s(p_1)$ (dark blue), $W^s(p_2^{\pm})$ (light blue), $W^u(p_1)$ (red), and $W^u(p_2)$ (purple), respectively. Panels (a)–(f) are for $\lambda = 0.8$, $\lambda = 0.78$, $\lambda = 0.779129$, $\lambda = 0.75$, $\lambda = 0.7$ and $\lambda = 0.6$, respectively.

critical tangencies.

This complicated transition in the small interval $\lambda \in [0.89, 0.904]$ generates infinitely many saddle points, which lie dense in the closure of the unstable set $W^u(p_1)$; hence, we have indeed a chaotic attractor $\mathcal{A}$, which is the only attractor other than infinity.

Transition through the first saddle-node bifurcation

As for $c = 0$, the attractor $\mathcal{A}$ grows larger as λ decreases further and the saddle periodic points on $\mathcal{A}$ come closer to the repelling periodic points on $\mathcal{Y}$. Figure 5 shows phase portraits illustrating further changes in the dynamics of map (1) for six decreasing values of $\lambda \in [0.6, 0.8]$ in panels (a)–(f), respectively. Panels (a) and (b) are the phase portraits for $\lambda = 0.8$ and $\lambda = 0.78$, where the dynamics are qualitatively the same as in Figure 3(f), but the points p_1 and $p_2^{\pm}$ and their unstable sets $W^u(p_1)$ and $W^u(p_2)$ lie further away from J_0 and the point p_1 in $\mathcal{A}$ lies closer to the point s_1 in $\mathcal{Y}$. At $\lambda = (11 + \sqrt{21})/20 \approx 0.779129$, the fixed points p_1 and s_1 meet, as shown in Figure 5(c). In contrast to the case $c = 0$, this is not a transcritical bifurcation, but a saddle-node bifurcation. The chaotic attractor $\mathcal{A}$ meets its basin boundary $\mathcal{Y}$, but now only in the point $p_1 = s_1$. Note that the preimages of $p_1 = s_1$ lie in $\mathcal{Y}$, but not on the attractor $\mathcal{A}$.

After the saddle-node bifurcation, the fixed points p_1 and s_1 and the sets $W^s(p_1)$ and $W^u(p_1)$ have disappeared. Figures 5(d)–(f) show the dynamics for parameter values $\lambda \in (0.3208, 0.779129)$, after the saddle-node bifurcation, with phase portraits for $\lambda = 0.75$, $\lambda = 0.7$ and $\lambda = 0.6$, respectively. Now that p_1 is gone, the unstable set $W^u(p_2)$ and the forward critical set $\mathcal{J}^+$ are no longer bounded by $W^u(p_1)$. Instead, $W^u(p_2)$ and $\mathcal{J}^+$ intersect the Julia set $\mathcal{Y}$ and the basin $\mathcal{B}(\infty)$, which means that they are now unbounded. Hence, the closure of the saddle periodic points is not a chaotic attractor, but a chaotic saddle, which we denote by $\mathcal{S}$. The critical circle J_1 contains points that go to infinity, for example, the point $c + 1 - \lambda$, and points that stay bounded under iteration of map (1), for example $W^s_0(p_2^{\pm}) \cap J_1$. Therefore, J_1 must also contain points that lie in $\mathcal{Y}$; note that J_0 now lies in $\mathcal{Y}$ as well.

Before we discuss the Julia set $\mathcal{Y}$ in this parameter regime, let us first study the effect of the saddle-node bifurcation on the stable and unstable sets $W^s(p_1)$ and $W^u(p_1)$ and the saddle periodic points in more detail.

Details of the first saddle-node bifurcation

Figure 6 shows the phase portraits for $\lambda = 0.8$ in column (a), $\lambda = 0.779129$ in column (b) and $\lambda = 0.75$ in column (c) before, approximately at, and after the saddle-node bifurcation, respectively. The top row shows the fixed points p_1 and s_1, the stable sets $W^s(p_1)$ and $W^s(p_2^{\pm})$, the critical point J_0 and the Julia set $\mathcal{Y}$ in the positive quadrant of the complex plane; the bottom row shows J_0, J_1, the unstable set $W^u(p_1)$ and all saddle periodic points up to period 15. Before the bifurcation, as shown in panel (a1), the primary branch $W^s_0(p_1)$ contains p_1, extends to J_0 on one side and to s_1 on $\mathcal{Y}$ on the other. The saddle periodic points are dense in the chaotic attractor $\mathcal{A}$ and the unstable set $W^u(p_1)$ accumulates on $\mathcal{A}$; see panel (a2). The set $\mathcal{C}$ is the basin $\mathcal{B}(\mathcal{A})$, which is open and connected and its boundary $\mathcal{Y}$ is a Jordan curve.

At the saddle-node bifurcation of p_1 and s_1, the preimages of p_1 in $W^s(p_1)$ are equal to the preimages of s_1 in $\mathcal{Y}$. Here, $\mathcal{C}$ is still $\mathcal{B}(\mathcal{A})$ and $\mathcal{Y}$ is still a Jordan curve; see panel (b1). The fixed point $p_1 = s_1$ has one eigenvalue at 1 and, therefore, the contraction to p on $W^s(p)$ is no longer exponential. The point p_1 lies on the attractor $\mathcal{A}$ and the point s_1 lies on its basin boundary $\mathcal{Y}$, so this bifurcation is a boundary crisis of $\mathcal{A}$; see [McDonald *et al.*(1985a), McDonald *et al.*(1985b)] for more details on boundary crisis of fractal basin boundaries.

After the saddle-node bifurcation, the stable set $W^s(p_1)$ has disappeared together with p_1 and s_1; see panel (c1). Furthermore, the chaotic attractor $\mathcal{A}$ and its basin $\mathcal{B}(\mathcal{A})$ have disappeared; see panel (c2). Points on the entire positive real line and its preimages (grey curves) now go to infinity, while $W^s(p_2^{\pm})$ stays bounded under iteration of (1). The closure of the saddle periodic points forms the chaotic saddle $\mathcal{S}$ that induces *transient chaos* [Kaplan & Yorke(1979)]: immediately after the bifurcation, the set $\mathcal{S}$ is chaotic and orbits of points in the former basin $\mathcal{B}(\mathcal{A})$ are initially all attracted by $\mathcal{S}$, but eventually most diverge to infinity.

After the bifurcation, map (1) has no attractor and the set $\mathcal{C} = \mathbb{C} \backslash (\mathcal{B}(\infty) \cup \mathcal{Y})$ is empty. However, the closures of $W^s(p_2^{\pm})$ and the stable sets of all other saddle periodic points stay bounded under iteration and, hence, must be contained in $\mathcal{Y}$. On the other hand, the closure of the stable sets consists of infinitely many arcs that have the pre-periodic repelling points as their end points. Therefore, we conclude that $\mathcal{Y}$ now coincides with the closure of the stable sets of all saddle points. This means that $\mathcal{Y}$ is compact, connected and does not contain any Jordan curves. Furthermore, it is locally connected only in the point J_0, so it is not a dendrite. Note that this is the first time that the Julia set of map (1) is neither a union of Jordan curves, nor a Cantor set, nor a dendrite. All together, our numerical investigations suggest, that $\mathcal{Y}$ is a so-called *Cantor bouquet*. This is an infinite union of arcs that emanate from one point, such that the end points of these arcs are dense in the set [Aarts & Oversteegen(1993), Bula & Oversteegen(1990)]. The Cantor bouquet is locally connected only at the point of connection of the arcs, which is J_0 in this case. Furthermore, the set of end points of the arcs together with the point of connection of the arcs is a connected set, whereas the set without this point is totally disconnected; such a point is called an *explosion point* [Mayer(1990)]. Cantor bouquets have been found in the study of Julia sets of the exponential map $z \mapsto \lambda \exp(z)$ for $\lambda < e^{-1}$, where the explosion point is at infinity; see [Aarts & Oversteegen(1993), Bula & Oversteegen(1990), Devaney & Krych(1984), Krauskopf & Kriete(1998), Mayer(1990)] for more details.

Transition through a second saddle-node bifurcation of p_1

As λ decreases further, the fixed points p_1 and s_1 and the sets $W^s(p_1)$ and $W^u(p_1)$ reappear in a second saddle-node bifurcation, which induces the transition shown in Figure 5, but in reverse order. Figure 7 shows changes in the phase portraits for six decreasing values of $\lambda \in [0, 0.4]$ in panels (a)–(f). Note that panels (a)–(d) are shown

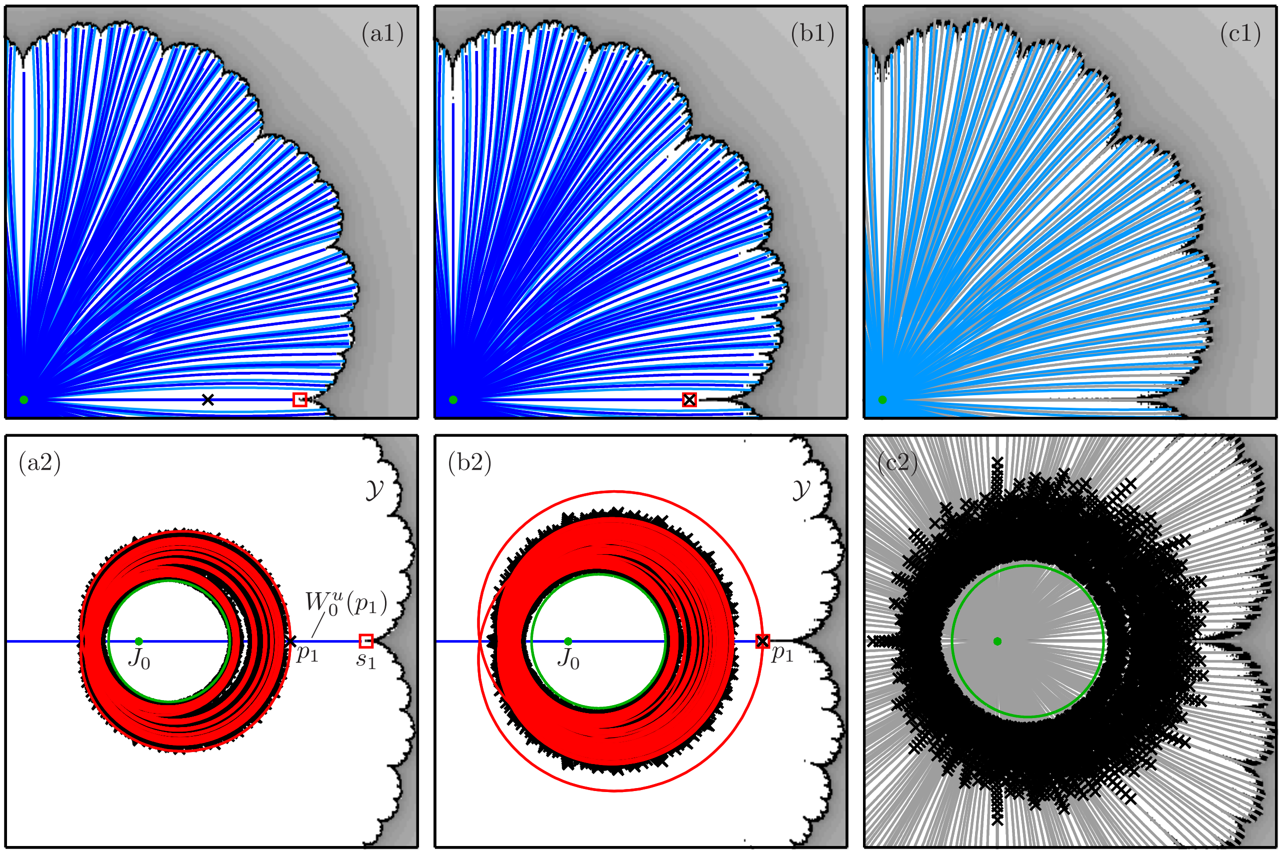

Figure 6: The effect of the saddle-node bifurcation of the fixed points p_1 and s_1 at $\lambda = 0.779129$; the top row shows J_0 (green), the saddle point p_1 (black cross), the repellor s_1 (red square), the stable sets $W^s(p_1)$ (blue) and $W^s(p_2^{\pm})$ (light blue) and the Julia set $\mathcal{Y}$; the bottom row shows the critical point J_0 (green), the critical circle J_1 (green), all saddle periodic points up to period 15 and the unstable set $W^u(p_1)$ (red). The parameter values are $c = 0.1$ and $\lambda = 0.8$ before the bifurcation in column (a), $\lambda = 0.779129$ approximately at the bifurcation in column (b) and $\lambda = 0.75$ after the bifurcation in column (c).

in the range $[-2.5, 2.5] \times [-2.5, 2.5]$, whereas panels (e) and (f) are shown in the range $[-4.3, 4.3] \times [-4.3, 4.3]$, because the basin $\mathcal{B}(\mathcal{A})$ extends in the course of the transition, as was the case for $\lambda < 0.5$ and $c = 0$. Panels (a) and (b) show the situation at $\lambda = 0.4$ and $\lambda = 0.35$, respectively, where the dynamics are qualitatively the same as in Figures 5(d)–(f): there are no fixed points, $W^u(p_2)$ is unbounded and we believe that the Julia set $\mathcal{Y}$ is a Cantor bouquet with explosion point J_0. Panel (c) is the phase portrait for $\lambda = 0.3208$, approximately at the second saddle-node bifurcation at which p_1, s_1 and the chaotic attractor $\mathcal{A}$ reappear; compare with Figure 5(c). Figures 7(d) and (e) are the phase portraits for $\lambda = 0.3$ and $\lambda = 0.2$, after the second saddle-node bifurcation; compare with Figures 5(b) and (a).

Figure 7(f) is the phase portrait for $\lambda = 0$, where map (1) reduces to (5) for $c = 0.1$; compare with Figure 2(f). As for $c = 0$, the stable set $W^s(p_1)$ and $W^s(p_2^{\pm})$ are straight lines, which extend from J_0 to infinity, each point in these sets immediately maps to p_1 and $p_2^{\pm}$, respectively, and the chaotic attractor $\mathcal{A}$ (magenta) is the critical circle J_1, but now J_1 is centred around $c = 0.1$. Saddle periodic points still seem to be dense in $\mathcal{A}$ and, therefore, we believe that (1) restricted to $\mathcal{A}$ for $c = 0.1$ is a one-dimensional chaotic map that is topologically equivalent to the angle-doubling map on the unit circle.

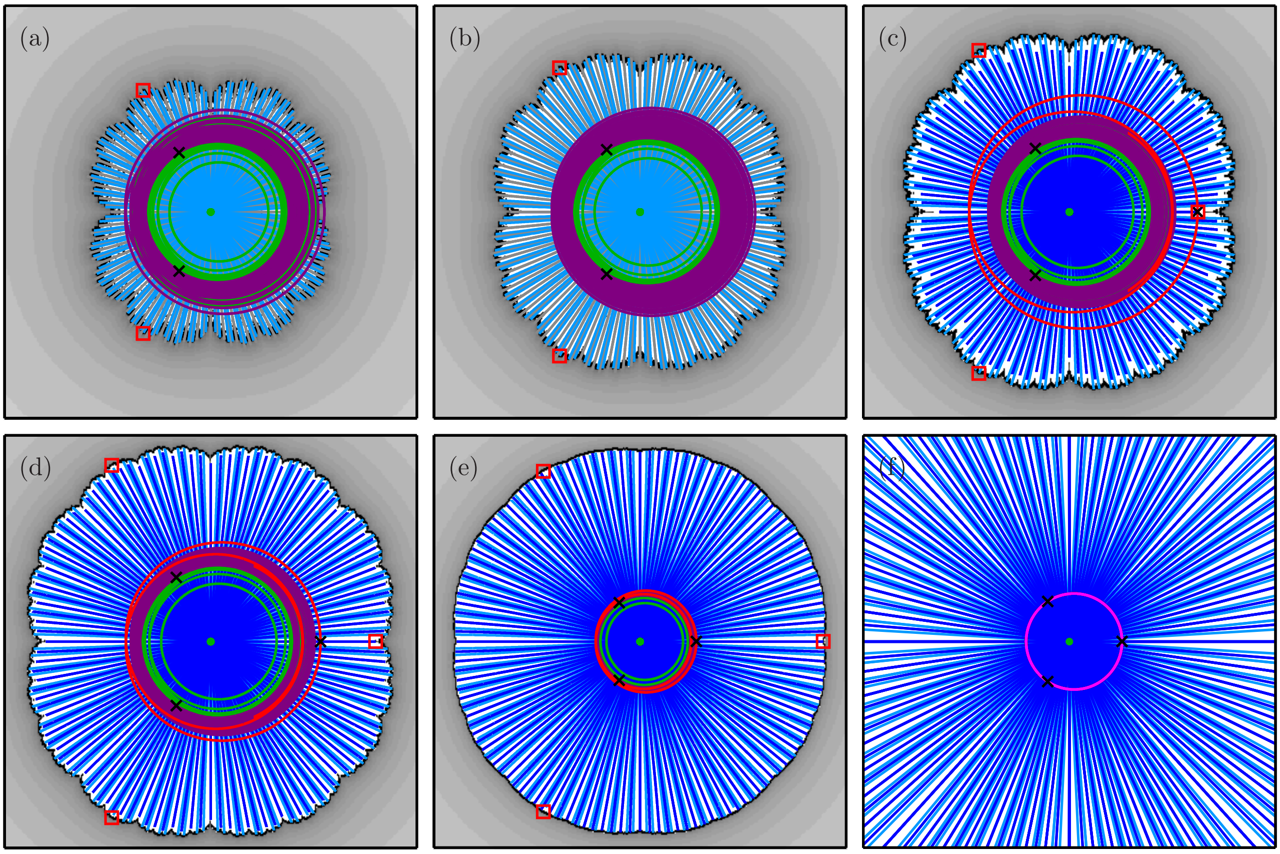

Figure 7: Last step in the transition of the phase portrait for $c = 0.1$ in $[-2.5, 2.5] \times [-2.5, 2.5]$ (panels (a)–(d)) or $[-4.3, 4.3] \times [-4.3, 4.3]$ (panels (e)–(f)); shown are the Julia set $\mathcal{Y}$ (black), the critical set $\mathcal{J}$ (green), the fixed points p_1 (black cross) and s_1 (red square), the period-two points $p_2^{\pm}$ (black crosses) and $s_2^{\pm}$ (red squares), and their stable and unstable sets $W^s(p_1)$ (dark blue), $W^s(p_2^{\pm})$ (light blue), $W^u(p_1)$ (red), and $W^u(p_2)$ (purple), respectively. Panels (a)–(f) show phase portraits for $\lambda = 0.4$, $\lambda = 0.35$, $\lambda = 0.3208$, $\lambda = 0.3$, $\lambda = 0.2$ and $\lambda = 0$, respectively.

3.3 Global transitions for $c = -0.25$

We now consider an orientation-reversing case, namely, we choose $c = -0.25$ to the left of the centre in the main cardioid of $\mathcal{M}$. Some of these results were also part of the MEng project by Madeleine Jones at the University of Bristol. For $c = -0.25$ and $\lambda \in [0, 1]$ decreasing from 1 for map (1), we encounter a similar sequence of bifurcations as for $c = 0.1$ in Section 3.2. However, the transition is preceded by a period-doubling bifurcation and the sequence of bifurcations described in Section 3.2 occurs for the emanating period-two orbit instead of the fixed point. We start with the phase portrait of (1) for $\lambda = 1$ in Figure 8(a). As for $c = 0.1$, the map has an attracting fixed point p_1 (blue triangle) and a repelling fixed point s_1 (red square) on the real line, the Julia set $\mathcal{Y}$ (black) is a Jordan curve bounding the basin $\mathcal{B}(p_1) = \mathcal{C}$, the backward critical set $\mathcal{J}^-$ (green dots) accumulates on $\mathcal{Y}$ and the forward critical set $\mathcal{J}^+$ (green dots) accumulates on p_1; compare with Figure 3(a). Note that, p_1 now lies on the negative real line and the points J_{-1}^0 and J_{-1}^1 and infinitely many higher-order preimages of the critical point J_0 in $\mathcal{J}^-$ lie on the real line. Since the map is orientation reversing, the points $J_k \in \mathcal{J}^+$ lie to the right (left) of p_1 if $k > 0$ is even (odd).

As $\lambda < 1$, initially, J_1 becomes the circle with radius $1 - \lambda$ around $c = -0.25$ and the images of J_1 in $\mathcal{J}^+$ become closed curves accordingly but, otherwise, the phase portrait is unchanged; see Figure 8(b) for the phase portrait for $\lambda = 0.95$. As λ decreases further, the fixed point p_1 destabilises in a period-doubling bifurcation

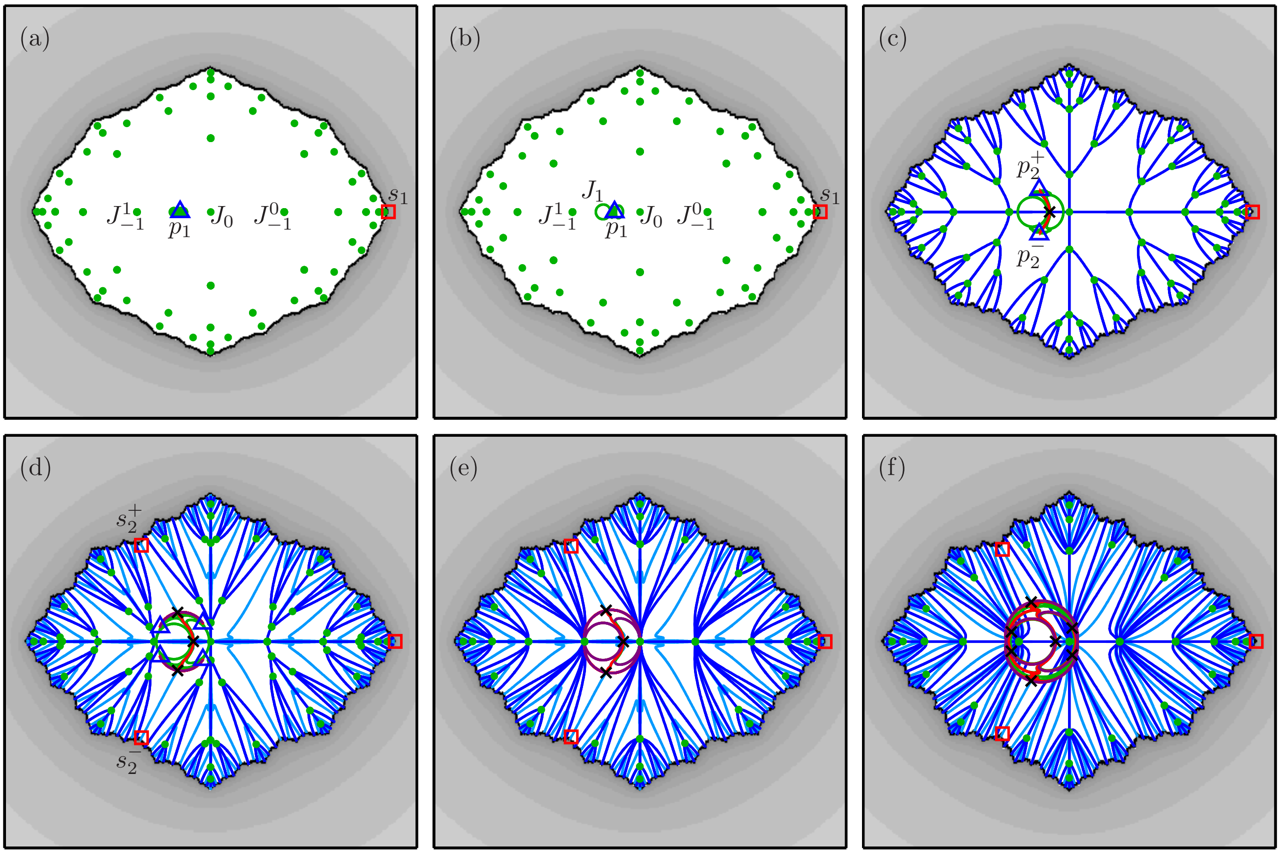

Figure 8: First step in the transition of the phase portrait for $c = -0.25$ in $[-1.4, 1.4] \times [-1.4, 1.4]$; shown are the Julia set $\mathcal{Y}$ (black), the critical set $\mathcal{J}$ (green), the fixed points p_1 (blue triangle/black cross) and s_1 (red square), the period-two points $p_2^\pm$ (blue triangles/black crosses), $q_2^\pm$ (blue triangles), $r_2^\pm$ (blue triangles) and $s_2^\pm$ (red squares), their stable and unstable sets $W^s(p_1)$ (dark blue), $W^s(p_2^\pm)$ (light blue), $W^u(p_1)$ (red), and $W^u(p_2)$ (purple), respectively, and the period-four points p_4^k, $1 \le k \le 4$ (black crosses). Panels (a)–(f) are for $\lambda = 1$, $\lambda = 0.95$, $\lambda = 0.9$, $\lambda = 0.88$, $\lambda = 0.8737$, and $\lambda = 0.85$, respectively.

at $\lambda \approx 0.94286$, where the period-two attractors $p_2^\pm$ are born and p_1 becomes a saddle fixed point. Figure 8(c) is the phase portrait for $\lambda = 0.9$, immediately after the period-doubling bifurcation. The saddle fixed point p_1 has one-dimensional stable and unstable sets $W^s(p_1)$ (blue) and $W^u(p_1)$ (red) and the two sides of $W^u(p_1)$ end at p_2^+ and p_2^-. Similar to what happened after the pitchfork bifurcation for $c = 0.1$, the stable set $W^s(p_1)$ has a tree structure with the points in $\mathcal{J}^-$ as branch points. However, infinitely many points in $\mathcal{J}^-$ now lie on the real line; compare with Figure 3(c). The set $\mathcal{C}$ is the union of the sets $\mathcal{B}(p_2^\pm)$, $W^s(p_1)$ and $\mathcal{J}^-$.

As λ decreases further, the period-two points $p_2^\pm$ destabilise in a pitchfork bifurcation at $\lambda \approx 0.88993$, at which two pairs of period-two attracting points, denoted $q_2^\pm$ and $r_2^\pm$, are born. Figure 8(d) is the phase portrait for $\lambda = 0.88$, after the pitchfork bifurcation of $p_2^\pm$. The period-two points $p_2^\pm$ (black crosses) are saddles with one-dimensional stable and unstable sets $W^s(p_2^\pm)$ (light blue) and $W^u(p_2^\pm)$ (purple). As before, the stable set $W^s(p_2^\pm)$ consists of all preimages of the primary branches $W_0^s(p_2^\pm)$, which extend to the period-two repellors $s_2^\pm \in \mathcal{Y}$ on one side and to J_0 on the other. The two sides of $W^u(p_2^\pm)$ end at $q_2^\pm$ and $r_2^\pm$, respectively. The unstable set $W^u(p_1)$ accumulates on the closure of $W^u(p_2)$ and the circles in $\mathcal{J}^+$ accumulate on the closure of $W^u(p_1)$. However, typical points on $W^u(p_1)$ and J_1 (not on $W^s(p_2^\pm)$) are attracted by $q_2^\pm$ or $r_2^\pm$. The set $\mathcal{C}$ is the union of basins $\mathcal{B}(q_2^\pm)$ and $\mathcal{B}(r_2^\pm)$, the stable sets $W^s(p_1)$ and $W^s(p_2^\pm)$ and $\mathcal{J}^-$.

At $\lambda \approx 0.8738$, $W^u(p_2)$ and $W^s(p_1)$ become tangent in a first heteroclinic tangency and, shortly after, $W^u(p_2)$

and $\mathcal{J}^-$ become tangent in a first backward critical tangency. This bifurcation induces an infinite sequence of forward-backward critical tangencies, which leads to the appearance of infinitely many saddle periodic points via the mechanism we discussed for Figure 4.

Figure 8(e) is the phase portrait for $\lambda = 0.8737$, where J_0 lies on J_2 and J_{-1}^1 lies on J_1 in a forward-backward critical tangency. Similar to the forward-backward critical tangency for J_0 and J_1, the preimages of J_{-1}^1 have disappeared into J_0, but $\mathcal{J}^+$ still contains all preimages of J_{-1}^0. Here, the circles in $\mathcal{J}^+$ form two nested sets $J_k \subset J_{k+2}$ for all $k \in \mathbb{N}$, because $J_{-1}^1 \in J_1$and $J_0 \in J_2$. At the same time, the period-two attractors $q_2^\pm$ and $r_2^\pm$ disappear into J_0 and J_{-1}^1 and the unstable set $W^u(p_2)$ intersects itself. The sets $W^u(p_1)$ and $W^u(p_2)$ are bounded by the two closed segments of $W^u(p_2)$ containing $p_2^\pm$ up to their first intersection. Similar to the closure of $W^u(p_1)$ for $c = 0.1$, we believe that the closure of $W^u(p_2)$ for $c = -0.25$ is a chaotic attractor $\mathcal{A}$, that saddle periodic points lie dense in $\mathcal{A}$, and that the basin $\mathcal{B}(\mathcal{A})$ is the set $\mathcal{C}$; compare with Figure 6(b).

Figure 8(f) is the phase portrait for $\lambda = 0.85$, after the forward-backward critical tangency of J_0 and J_2. Four saddle period-four points p_4^k, $1 \leq k \leq 4$, (black crosses) have appeared near J_0 and J_{-1}^1. They have one-dimensional stable and unstable sets and corresponding repelling period-four points s_4^k in $\mathcal{Y}$ (not shown).

Transition through a pair of saddle-node bifurcations of $p_2^\pm$

For $c = -0.25$, map (1) undergoes two saddle-node bifurcations of the period-two saddle points $p_2^\pm$, at which the chaotic attractor $\mathcal{A}$ disappears and reappears. Figure 9 shows nine more phase portraits that illustrate the transition through these two saddle-node bifurcations. Note that we show ranges from $[-1.5, 1.5] \times [-1.5, 1.5]$ in panel (a) to $[-3.1, 3.1] \times [-3.1, 3.1]$ in panel (g) and $[-6.4, 6.4] \times [-6.4, 6.4]$ in panel (h), due to the expansion of the basin $\mathcal{B}(\mathcal{A})$. Panel (a) is the phase portrait for $\lambda = 0.81$, where the dynamics are qualitatively as in Figure 8(f), in the sense that the closure of $W^u(p_2)$ is the chaotic attractor $\mathcal{A}$, the saddle points p_1 and p_4^k, $1 \leq k \leq 4$, and their unstable sets lie on $\mathcal{A}$ and the basin $\mathcal{B}(\mathcal{A})$ is the set $\mathcal{C}$. Figure 9(b) is the phase portrait for $\lambda = 0.8$, where $p_2^\pm$ and $s_2^\pm$ meet in the first saddle-node bifurcation. As for the first saddle-node bifurcation of p_1 for $c = 0.1$, the chaotic attractor $\mathcal{A}$ hits its basin boundary $\mathcal{Y}$ in a boundary crisis, but here $\mathcal{A}$ and $\mathcal{Y}$ meet in the two points $p_2^\pm = s_2^\pm$.

Figure 9(c) is the phase portraits for $\lambda = 0.76$ after the saddle-node bifurcation of $p_2^\pm$ and $s_2^\pm$. The points $p_2^\pm$ and $s_2^\pm$, their stable and unstable sets $W^s(p_2^\pm)$ and $W^u(p_2^\pm)$, the chaotic attractor $\mathcal{A}$ and its basin of attraction $\mathcal{B}(\mathcal{A}) = \mathcal{C}$ have disappeared. Similar to what happened after the first saddle-node bifurcation for $c = 0.1$, the remaining sets $W^u(p_1)$ and $\mathcal{J}^+$ are now unbounded and intersect both $\mathcal{Y}$ and the basin $\mathcal{B}(\infty)$. Therefore, orbits of some points on J_1 stay bounded and orbits of other points on J_1 go to infinity. Since the intersection of J_1 and $\mathcal{Y}$ is now nonempty and $\mathcal{Y}$ is backward invariant and closed, J_0 and all its preimages in $\mathcal{J}^-$ now lie in $\mathcal{Y}$. As before $\mathcal{J}^-$ accumulates on $\mathcal{Y}$ and, hence, $\mathcal{J}^-$ is now a dense subset of $\mathcal{Y}$. At the same time, as for $c = 0.1$, the Julia set $\mathcal{Y}$ is the closure of the union of the stable sets of all saddle periodic points. However, our numerical calculations suggest that $\mathcal{Y}$ is not a Cantor bouquet: even though $\mathcal{Y}$ consists of infinitely many arcs, such that the set of end points of these arcs is dense, these arcs are locally connected at more than one point, namely, in the dense subset $\mathcal{J}^-$. Therefore, $\mathcal{Y}$ has a dense set of explosion points and we refer to this type of set as a *Cantor tangle*.

As λ decreases, J_0 enters J_1 in a forward-backward critical tangency at $\lambda = 0.72$, where all preimages of J_0 in $\mathcal{J}^-$ disappear into J_0. Figure 9(d) is the phase portrait for $\lambda = 0.7$ after this bifurcation. The Julia set $\mathcal{Y}$ is now a Cantor bouquet, because $\mathcal{Y}$ is the closure of $W^s(p_1)$, the branches of $W^s(p_1)$ are now all connected to J_0, and the set $\mathcal{J}^-$ of explosion points contains only the point J_0.

As λ decreases further, the period-four points p_4^k and s_4^k, $1 \leq k \leq 4$ disappear and reappear in a pair of saddle-node bifurcations at $\lambda \approx 0.6897$ and $\lambda \approx 0.3578$; Figure 9(e) is the phase portrait for $\lambda = 0.4$ between these bifurcations. In fact, as we will see in the bifurcation diagram in Section 5, in the course of this transition, (1) undergoes further pairs of saddle-node bifurcations of other saddle periodic points in $\mathcal{A}$. However, we do not include these points or the points p_4^k and s_4^k in the following phase portraits, because they do not contribute to changes in the dynamics of map (1).

Figure 9(f) is the phase portrait for $\lambda = 0.3077$, where the period-two points $p_2^\pm$ and $s_2^\pm$ and the chaotic attractor $\mathcal{A}$ reappear in a second saddle-node bifurcation of $p_2^\pm$. Here, the dynamics are qualitatively the same as in panel (b), in the sense that $\mathcal{A}$ meets its basin boundary $\mathcal{Y}$ in the points $p_2^\pm = s_2^\pm$ and the set $\mathcal{C}$ is the basin

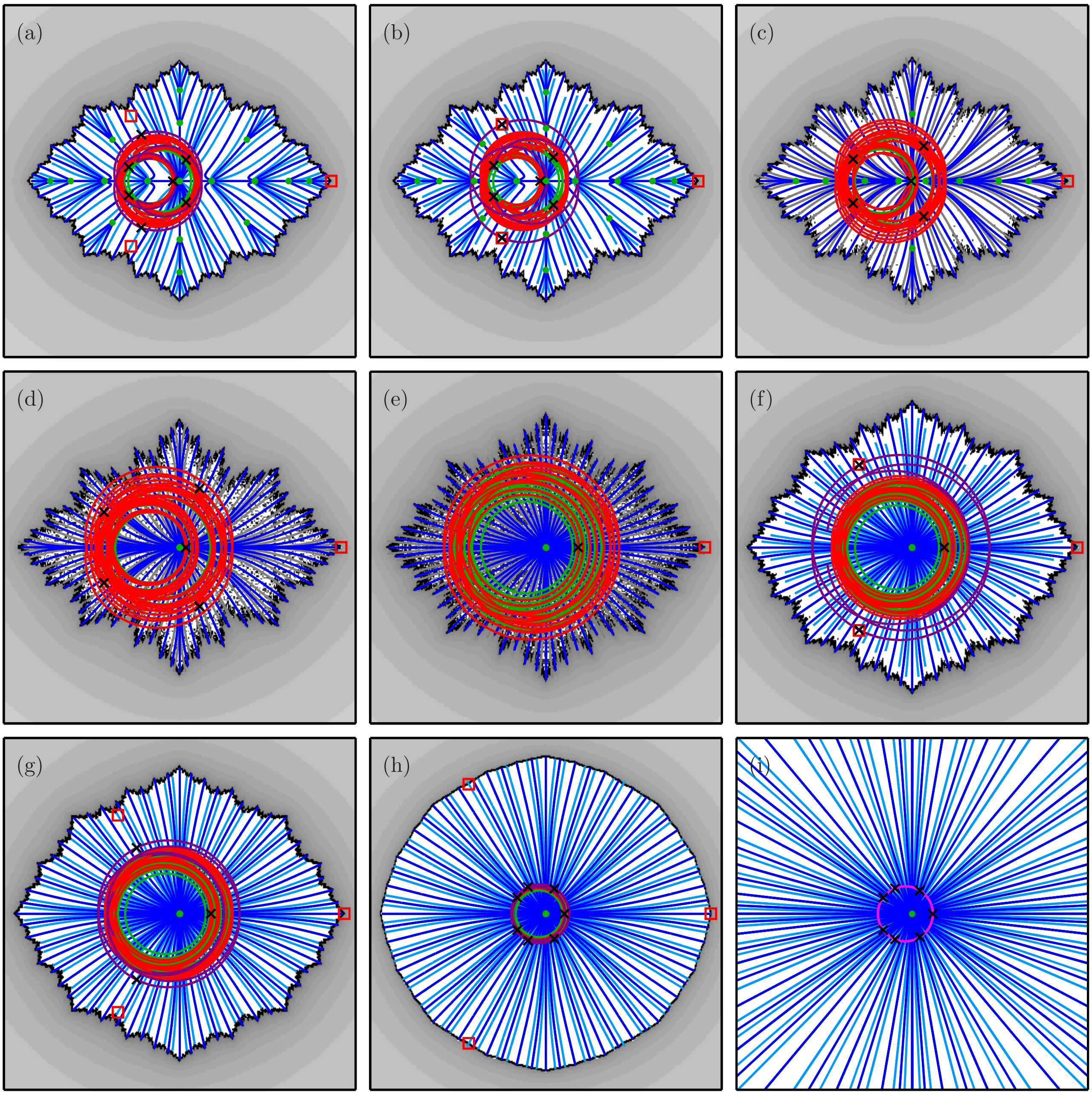

Figure 9: Last step in the transition of the phase portrait for $c = -0.25$ in $[-1.5, 1.5] \times [-1.5, 1.5]$ (panels (a)–(d)), $[-2.3, 2.3] \times [-2.3, 2.3]$ (panel (e)), $[-2.9, 2.9] \times [-2.9, 2.9]$ (panel (f)) and $[-3.1, 3.1] \times [-3.1, 3.1]$ (panel (g)) and $[-6.4, 6.4] \times [-6.4, 6.4]$ (panels (h)–(i)); shown are the Julia set $\mathcal{Y}$ (black), the critical set $\mathcal{J}$ (green), the fixed points p_1 (black cross) and s_1 (red square), the period-two points $p_2^{\pm}$ (black crosses) and $s_2^{\pm}$ (red squares), their stable and unstable sets $W^s(p_1)$ (dark blue), $W^s(p_2^{\pm})$ (light blue), $W^u(p_1)$ (red), and $W^u(p_2)$ (purple), respectively, and the period-four points p_4^k, $1 \leq k \leq 4$ (black crosses). Panels (a)–(f) are for $\lambda = 0.81$, $\lambda = 0.8$, $\lambda = 0.76$, $\lambda = 0.7$, $\lambda = 0.4$, $\lambda = 0.3077$, $\lambda = 0.29$, $\lambda = 0.15$ and $\lambda = 0$, respectively.

of attraction $\mathcal{B}(\mathcal{A})$. Figures 9(g) and (h) are the phase portraits for $\lambda = 0.29$ and $\lambda = 0.15$ after the second saddle-node bifurcation of $p_2^{\pm}$ and $s_2^{\pm}$, respectively. Compared with panel (f), the points $p_2^{\pm}$ and $s_2^{\pm}$, and the sets $\mathcal{A}$ and $\mathcal{Y}$ lie further apart.

Finally, Figure 9(i) is the phase portrait for $\lambda = 0$, where, as for $c = 0$ and $c = 0.1$, the chaotic attractor $\mathcal{A}$ is the critical circle J_1, the stable sets $W^s(p_1)$ and $W^s(p_2^{\pm})$ are straight lines from J_0 to infinity and the Julia set $\mathcal{Y}$ is infinity.

4 The parameter c outside the Mandelbrot set $\mathcal{M}$

In this section we consider an orientation-preserving case outside $\mathcal{M}$, but close to the boundary of $\mathcal{M}$, namely the value $c = 0.28$. As before, we decrease $\lambda \in [0, 1]$ from $\lambda = 1$.

4.1 Global transitions for $c = 0.28$

Figure 10(a) shows the phase portrait of map (1) for $\lambda = 1$. Since $c = 0.28$ lies outside the Mandelbrot set $\mathcal{M}$, the Julia set $\mathcal{Y}$ (black) is a Cantor set, and the map has no attractor other than infinity. Therefore, the set $\mathcal{C} = \mathbb{C} \backslash (\mathcal{B}(\infty) \cup \mathcal{Y})$ is empty. The forward critical set $\mathcal{J}^+$ (green dots) consists of the images of the critical value $J_1 = 0.28$ and goes to infinity along the positive real line, whereas the backward critical set $\mathcal{J}^-$ (green dots) accumulates on $\mathcal{Y}$. The map has two complex-conjugate repelling fixed points q_1^+ and q_1^- (red squares) in $\mathcal{Y}$.

Figures 10(b) and (c) are the phase portraits for $\lambda = 0.95$ and $\lambda = 0.93$, respectively. The dynamics are qualitatively the same as in panel (a), but the critical circle J_1 is now a proper circle with radius $1 - \lambda > 0$. The set $\mathcal{J}^+$ consists of closed curves accordingly, and lies entirely in the basin $\mathcal{B}(\infty)$. Hence, $\mathcal{Y}$ is still a Cantor set. As λ is decreased further, the Julia set $\mathcal{Y}$ starts to interact with the forward critical set $\mathcal{J}^+$. It is difficult to find the value of λ that corresponds to the first interaction of $\mathcal{Y}$ and $\mathcal{J}^+$, because $\mathcal{Y}$ is a Cantor set before this interaction. However, after the bifurcation, $\mathcal{J}^-$ lies dense in $\mathcal{Y}$ and, therefore, this bifurcation is accumulated by an infinite sequence of forward-backward critical tangencies between $\mathcal{J}^+$ and $\mathcal{J}^-$. Figure 10(d) is the phase portrait for $\lambda = 0.92031$, where $\mathcal{J}^+$ and $\mathcal{J}^-$ meet in a forward-backward critical tangency that seems to be very close to the first interaction of $\mathcal{J}^+$ and $\mathcal{Y}$. At this parameter value, the point $J^s_{-17} \in \mathcal{J}^-$ lies on the critical circle J_1, where the sequence of preimages is $s = 10100010\dots0$, as defined in Section 2.4. We will discuss this bifurcation and its consequences for the Julia set $\mathcal{Y}$ and the backward critical set $\mathcal{J}^-$ in more detail in Figure 11.

Figure 10(e) is the phase portrait for $\lambda = 0.91$ after the forward-backward critical tangency between $J^s_{-17} \in \mathcal{J}^-$ and J_1. Large subsets of $\mathcal{Y}$ and $\mathcal{J}^-$ are enclosed by circles in $\mathcal{J}^+$. Therefore, orbits of some points in the disk enclosed by J_1 stay bounded and orbits of other points go to infinity. Since $\mathcal{Y}$ is closed and backward invariant, J_0 and all its preimages in $\mathcal{J}^-$ lie in $\mathcal{Y}$. Moreover, $\mathcal{J}^-$ still accumulates on $\mathcal{Y}$ and so the backward critical set $\mathcal{J}^-$ is dense in $\mathcal{Y}$. Furthermore, (1) has infinitely many saddle periodic points (not shown) that were born in the infinite sequence of forward-backward critical tangencies after the first interaction of $\mathcal{Y}$ and $\mathcal{J}^-$. These saddle periodic points and their stable sets must lie in $\mathcal{Y}$, because the set $\mathcal{C}$ is empty. Therefore, as for $c = -0.25$ between the first saddle-node bifurcation and the last backward critical tangency, the Julia set $\mathcal{Y}$ is a Cantor tangle with a dense set $\mathcal{J}^-$ of explosion points.

As λ is decreased further, the fixed points $q_1^{\pm}$ undergo a Neimarck–Sacker bifurcation at $\lambda \approx 0.89287$, where they become attractors. Figure 10(f) is the phase portrait at $\lambda = 0.89$, after this bifurcation. The set $\mathcal{C}$ (white) is the union of the basins $\mathcal{B}(q_1^{\pm})$, which are formed by all preimages of the immediate basins $\mathcal{B}_0(q_1^{\pm})$. Since $\mathcal{B}_0(q_1^{\pm})$ are bounded by Jordan curves, the boundary $\mathcal{Y}$ of $\mathcal{C}$ is now the closure of a union of infinitely many Jordan curves. We believe that $\mathcal{Y}$ is still connected, because $\mathcal{Y}$ was connected before this bifurcation and the bifurcation "replaces" every point in a dense subset of in $\mathcal{Y}$ with a Jordan curve. The infinitely many saddle periodic points can neither lie in the basins $\mathcal{B}(q_1^{\pm})$ nor in the basin $\mathcal{B}(\infty)$. Hence, they and their stable sets must still lie in $\mathcal{Y}$. All together, the numerical evidence suggests that $\mathcal{Y}$ shares some properties with the Julia set for bounded $\mathcal{J}^+$, for example, it is the closure of a union of Jordan curves, but it also shares some properties with the Cantor tangle, for example, $\mathcal{J}^-$ is dense in $\mathcal{Y}$. Therefore, $\mathcal{Y}$ can be thought of as a "Cantor tangle" containing a dense set of Jordan curves that bound the basins of finite attractors and we refer to this type of set as a *Cantor cheese*. It is unclear to us if the bounded components of $\mathcal{B}(\infty)$, for example, the open region near the imaginary axis between J_0 and J^0_{-1}, are bounded by Jordan curves. If this was the case then the Julia

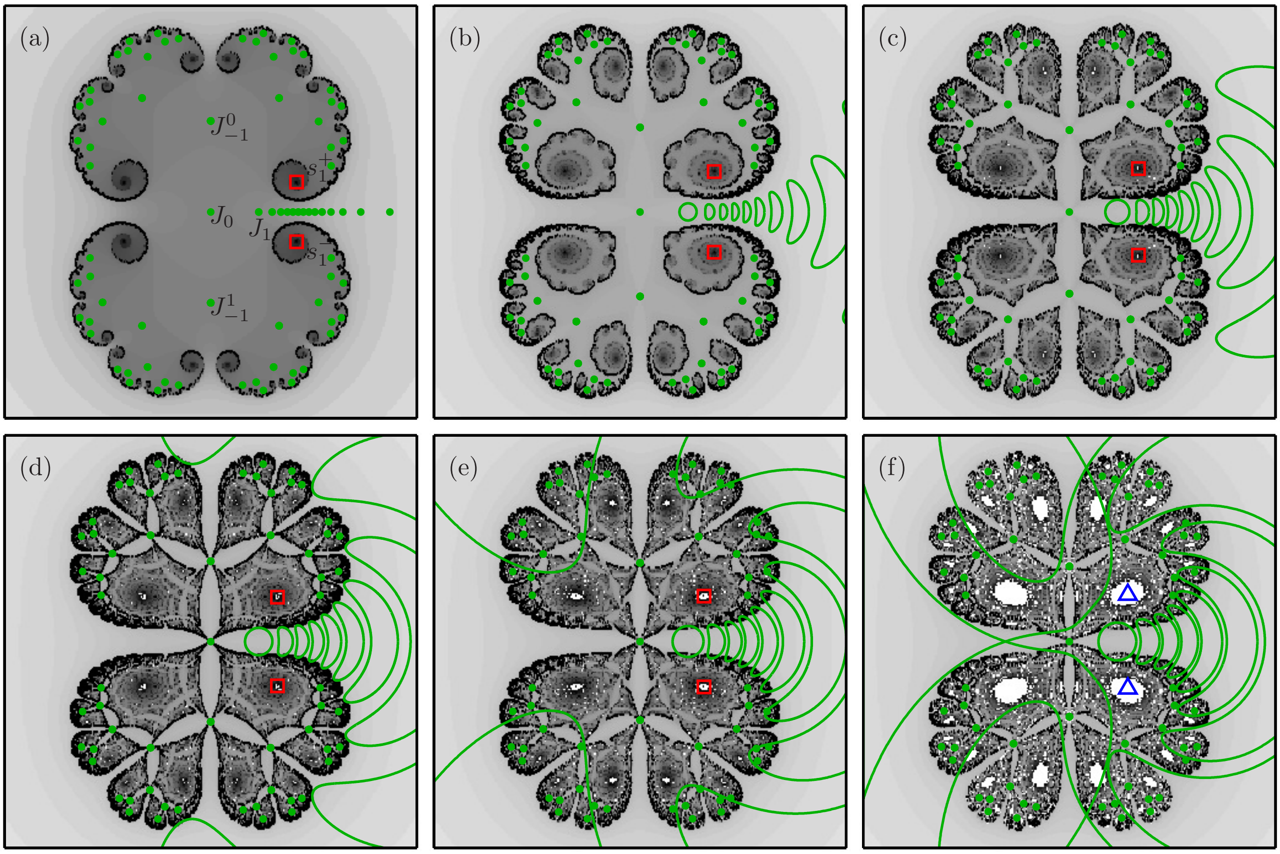

Figure 10: First step in the transition of the phase portrait for $c = 0.28$ in $[-1.2, 1.2] \times [-1.2, 1.2]$; shown are the Julia set $\mathcal{Y}$ (black), the critical set $\mathcal{J}$ (green) and the fixed points $q_1^{\pm}$ (red squares/blue triangles). Panels (a)–(f) are for $\lambda = 1$, $\lambda = 0.95$, $\lambda = 0.93$, $\lambda = 0.92031$, $\lambda = 0.91$, and $\lambda = 0.89$, respectively.

set could be a *Sierpinski carpet* or a *Sierpinski gasket*. As mentioned earlier, these types of Julia sets have been found in the study of singular perturbations of the complex quadratic map, namely, for the maps $z \mapsto z^2 + \alpha/z^m$ for $m = 1, 2$ [Devaney(2013), Blanchard *et al.*(2005), Marotta(2008)]. A more detailed study of the topology of the Julia set $\mathcal{Y}$ of (1) in this parameter regime lies beyond the scope of this paper.

Details of the forward-backward critical tangency

We now look closer at the changes of the Julia set $\mathcal{Y}$ and the backward critical set $\mathcal{J}^-$ induced by the forward-backward critical tangency of J_1 and J^s_{-17} at $\lambda = 0.92031$ with $s = 10100010\ldots0$; compare panels (c)–(e) in Figure 10. Figure 11 shows images before the bifurcation in column (a), approximately at the bifurcation in column (b), and after the bifurcation in column (c), namely for $\lambda = 0.925$, $\lambda = 0.92031$ and $\lambda = 0.915$, respectively. The top row shows $\mathcal{Y}$ (black), J_1 (green), $\mathcal{J}^-$ (green) and J^s_{-17} (dark green) and the bottom row shows, in addition, J_0 and J^{0s}_{-18} (dark green). Column (a) is the phase portrait for $\lambda = 0.925$ before the bifurcation; panel (a1) illustrates that the point J^s_{-17} and the rest of $\mathcal{J}^-$ lie outside critical circle J_1; panel (a2) shows that the first preimage J^{0s}_{-18} of J^s_{-17} and the rest of $\mathcal{J}^-$ lie correspondingly away from J_0. Column (b) is the phase portrait for $\lambda = 0.92031$, approximately at the bifurcation; the point J^s_{-17} lies on J_1 and J^{0s}_{-18} has disappeared into J_0 accordingly. At the same time, two repelling period-18 points $s^{\pm}_{18} \in \mathcal{Y}$ have disappeared into J_0 (not shown); this means that J_0 now lies in $\mathcal{Y}$ and, therefore, also in the closure of $\mathcal{J}^-$. Column (c) is the phase portrait for $\lambda = 0.915$ after the bifurcation; the point J^s_{-17} and a neighbourhood containing other points in $\mathcal{J}^-$ as well as points in $\mathcal{Y}$, lie well inside the disk bounded by J_1; see panel (c1). In particular, this

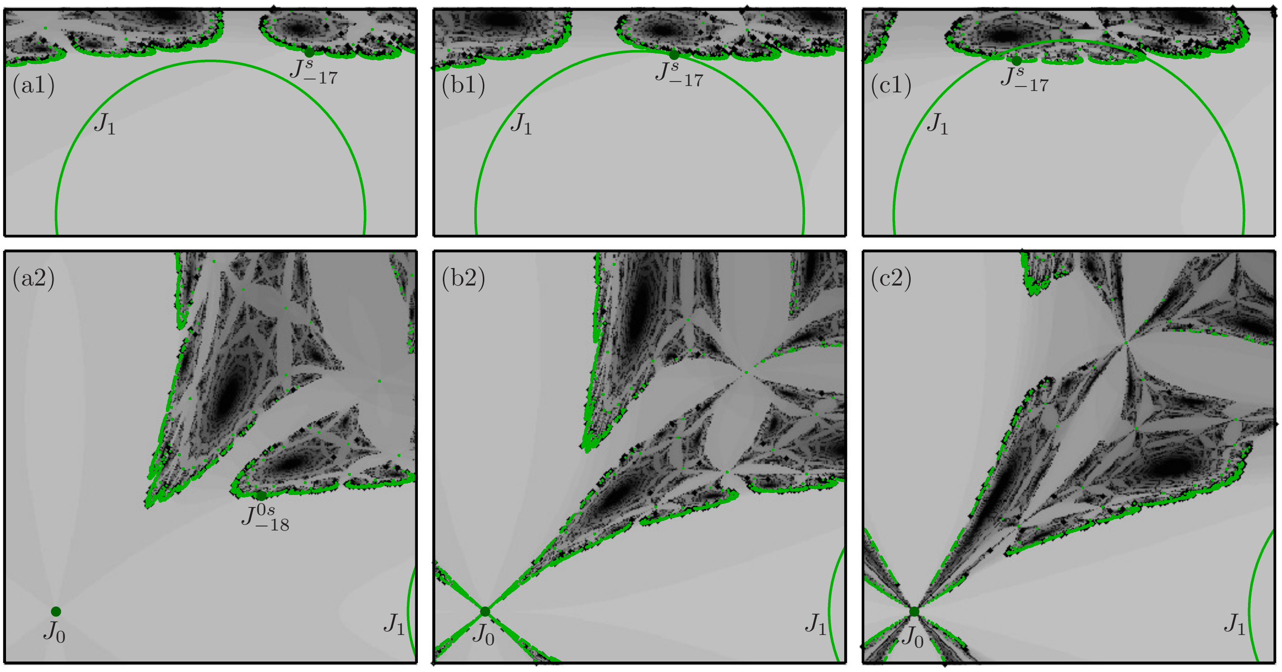

Figure 11: The effect of the forward-backward critical tangency of the critical circle J_1 and a point in the backward critical set $\mathcal{J}^-$ at $\lambda = 0.92031$; the top row shows the Julia set $\mathcal{Y}$ (black), the backward critical set $\mathcal{J}^-$, the critical circle J_1 (green), the point $J^s_{-17} \in \mathcal{J}^-$ (dark green), where $s = 10100010\ldots0$; the bottom row shows the Julia set $\mathcal{Y}$ (black), the backward critical set $\mathcal{J}^-$ (green), the critical point J_0 (dark green), the point $J^{0s}_{-18} \in \mathcal{J}^-$ (dark green) and the critical circle J_1 (green). The parameter values are $c = 0.28$ and $\lambda = 0.925$ before the bifurcation in column (a), $\lambda = 0.92031$ approximately at the bifurcation in column (b) and $\lambda = 0.915$ after the bifurcation in column (c).

neighbourhood no longer has a preimage; see panel (c2). As a result, the Julia set $\mathcal{Y}$ is no longer the closure of repelling periodic points, but it is still the closure of the periodic and pre-periodic repelling points. Recall, that we computed $\mathcal{Y}$ by plotting up to the third preimage of approximately three thousand repelling periodic points.

Transition through the last forward-backward critical tangency and a saddle-node bifurcation

In Figure 12 we show six more phase portraits that illustrate the changes in the dynamics of map (1) for $c = 0.28$ when λ is decreased further. Panel (a) is the phase portrait for $\lambda = 0.8$, where the dynamics are qualitatively as in Figure 10(f), but the basins $\mathcal{B}(q_1^{\pm})$ have expanded. Figure 12(b) is the phase portrait for $\lambda = 0.72$, at the last forward-backward critical tangency, where J_0 lies on J_1. At the same time, the attractors $q_1^{\pm}$, their basins $\mathcal{B}(q_1^{\pm})$, and the preimages of J_0 in $\mathcal{J}^-$ disappear into J_0. Therefore, $\mathcal{C}$ is empty, $\mathcal{Y}$ is the closure of the stable sets of all saddle periodic points, and the only explosion point is J_0; hence, the Julia set $\mathcal{Y}$ is a Cantor bouquet.

As λ is decreased further, the dynamics of map (1) undergoes a similar transition as for $c = 0.1$ and $\lambda < 0.5$, namely, there is a saddle-node bifurcation leading to the appearance of a saddle fixed point p_1 and a chaotic attractor $\mathcal{A}$; compare with Figure 5. Figures 12(c)–(d) are the phase portraits for $\lambda = 0.7$ and $\lambda = 0.3$, after the forward-backward critical tangency of J_0 and J_1, but before the saddle-node bifurcation of p_1. Map (1) has two period-two saddle points $p_2^{\pm}$ (black crosses) with stable and unstable sets $W^s(p_2^{\pm})$ (light blue) and $W^u(p_2)$ (purple), respectively; the Julia set $\mathcal{Y}$ is a Cantor bouquet.

Figures 12(e) and (f) are the phase portraits for $\lambda = 0.2405$ and $\lambda = 0.2$, that is, approximately at and after the saddle-node bifurcation of p_1, respectively. The dynamics is qualitatively as that at and after the second saddle-node bifurcation for $c = 0.1$, respectively, in the sense that the stable set $W^s(p_1)$ is formed by straight

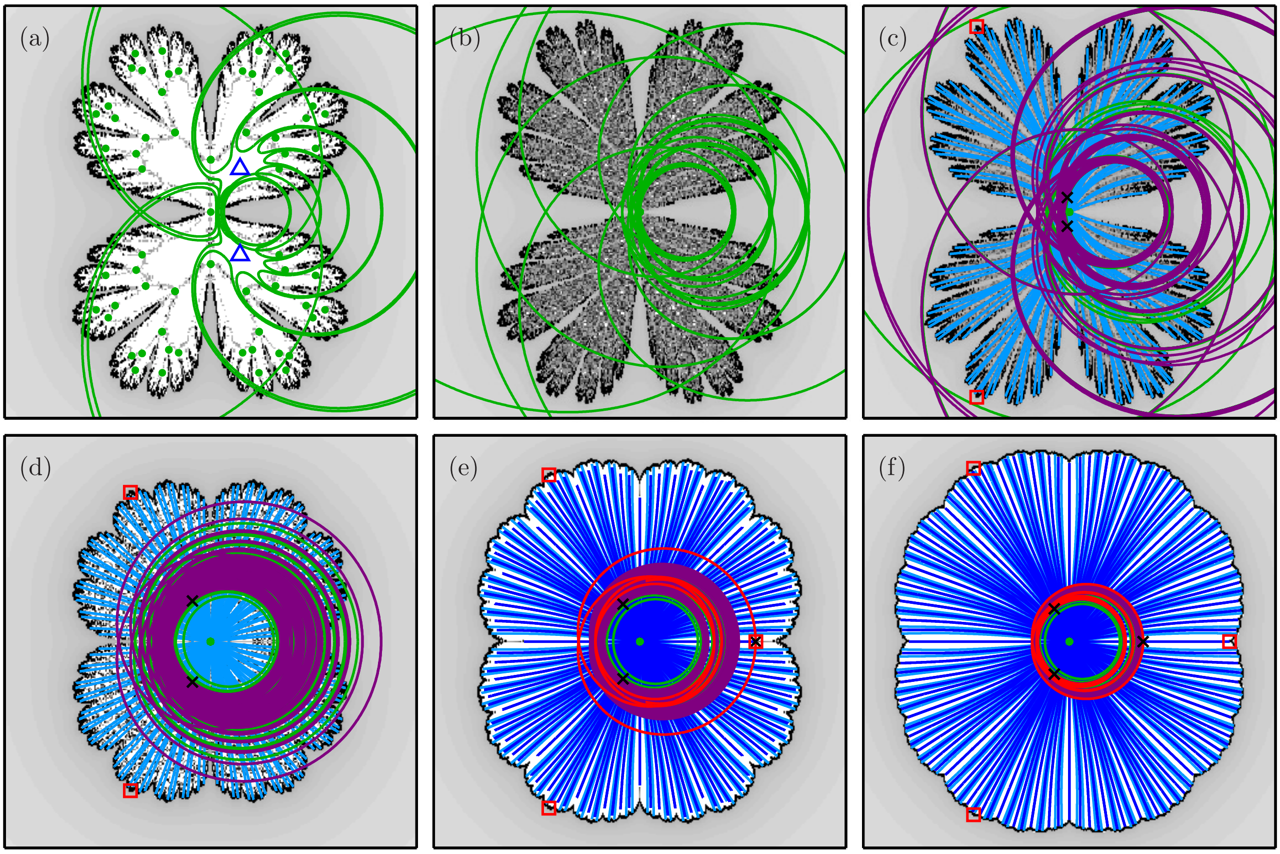

Figure 12: Last step in the transition of the phase portrait for $c = 0.28$ in $[-1.25, 1.25]\times[-1.25, 1.25]$ (panels (a)–(c)), $[-3.2, 3.2]\times[-3.2, 3.2]$ (panel (d)), $[-3.7, 3.7]\times[-3.7, 3.7]$ (panel (e)) and $[-4.4, 4.4]\times[-4.4, 4.4]$ (panel (f)), respectively; shown are the Julia set $\mathcal{Y}$ (black), the critical set $\mathcal{J}$ (green), the fixed points $q_1^{\pm}$ (blue triangles), p_1 (black cross) and s_1 (red square), the period-two points $p_2^{\pm}$ (black crosses) and $s_2^{\pm}$ (red squares), and their stable and unstable sets $W^s(p_1)$ (dark blue), $W^s(p_2^{\pm})$ (light blue), $W^u(p_1)$ (red), and $W^u(p_2)$ (purple), respectively. Panels (a)–(f) are for $\lambda = 0.8$, $\lambda = 0.72$, $\lambda = 0.7$, $\lambda = 0.3$, $\lambda = 0.2405$ and $\lambda = 0.2$, respectively.

lines from J_0 to s_1 and its preimages in $\mathcal{Y}$, the closure of $W^u(p_1)$ forms a chaotic attractor $\mathcal{A}$ and saddle periodic points are dense in $\mathcal{A}$.

We do not show the phase portrait at $\lambda = 0$, because it is qualitatively the same as for $c = 0$, $c = 0.1$ and $c = -0.25$, that is, $\mathcal{Y}$ is only the point infinity, the chaotic attractor $\mathcal{A}$ is the circle J_1 and the stable sets consist of straight lines extending from J_0 to infinity; see Figures 2(f), 7(f) and 9(h).

5 Bifurcation diagram in the $(\mathrm{Re}(c), \lambda)$-plane

In Sections 3 and 4 we discussed the transitions when decreasing $\lambda \in [0, 1]$ from $\lambda = 1$ for three different fixed values of c in the main cardioid of the Mandelbrot set $\mathcal{M}$ and one outside of $\mathcal{M}$. We now investigate how these individual transitions are linked to each other by also varying the parameter c, where we take $c \in \mathbb{R}$ as before. Hence, we study the bifurcation diagram of map (1) in the $(\mathrm{Re}(c), \lambda)$-plane with $\mathrm{Im}(c) = 0$ fixed.

We continue the bifurcations in two parameters using the method from [Hittmeyer *et al.*(2013)]. This method is an adaptation of the boundary value setup in [Beyn & Kleinkauf(1997)] for following homoclinic or heteroclinic tangencies, which is implemented it in Cl_MatContM [Dhooge *et al.*(2003), Ghaziani *et al.*(2009), Govaerts *et al.*(2008)]; our method also follows the three critical tangency bifurcations.

5.1 Bifurcation diagram near the main cardioid of $\mathcal{M}$

First, we consider $c \in \mathbb{R}$ in the range $[-0.75, 1.25]$, that is, inside the main cardioid of $\mathcal{M}$, for the segment $[-0.75, 0.25]$, and outside of $\mathcal{M}$ for $c > 0.25$. The value $c = 0.25$ corresponds to the saddle-node bifurcation S_1 at the cusp point on the boundary of the main cardioid, and $c = -0.75$ is the first period-doubling bifurcation P_1 on the boundary $\partial\mathcal{M}$ between the main cardioid and the period-two bulb of $\mathcal{M}$; see Figure 1. Figure 13 shows the bifurcation diagram of the map (1) in the $(\mathrm{Re}(c), \lambda)$-plane for $\mathrm{Re}(c) \in [-0.75, 1.25]$ and $\lambda \in [0, 1]$. We construct the bifurcation diagram in steps: panel (a) shows the bifurcations of the fixed points p_1, $q_1^{\pm}$ and s_1, of the period-two points $p_2^{\pm}$, $q_2^{\pm}$, $r_2^{\pm}$ and $s_2^{\pm}$, of the critical point J_0, and of the critical circle J_1 and its image J_2; panel (b) shows an enlargement of the bifurcation diagram in panel (a) in the range $(\mathrm{Re}(c), \lambda) \in [0.06, 0.36] \times [0.7, 1]$; and panel (c) shows the bifurcation diagram of panel (a) together with loci of saddle-node bifurcations of saddle points with higher periods and loci of forward-backward critical tangencies of J_0 with higher-order images of J_1 in $\mathcal{J}^+$.

The line $\lambda = 1$ in Figure 13(a) corresponds to the line $\mathrm{Im}(c) = 0$ in the bifurcation diagram of the complex quadratic family (2) in Figure 1(b); the points S_1, C_1 and P_1 on this line are the saddle-node bifurcation of p_1 and s_1 of (2) at $(0.25, 1)$, the centre of the main cardioid of $\mathcal{M}$ at $(0, 1)$, and the period-doubling bifurcation of p_1 at $(-0.75, 1)$, respectively. We also already considered slices along the lines $c = 0$, $c = 0.1$, $c = -0.25$ and $c = 0.28$ in Sections 3.1, 3.2, 3.3 and 4.1, respectively. The curve FB^1 (green) denotes the curve of last forward-backward critical tangencies, that is, of forward-backward critical tangencies of J_0 and J_1, and is given by $\{(\mathrm{Re}(c), \lambda) : \mathrm{Re}(c) = \pm(1 - \lambda)\}$. For $\mathrm{Re}(c) > 0$, the attractors $q_1^{\pm}$ exist for $(\mathrm{Re}(c), \lambda)$ above the curve FB^1 and the period-two saddles $p_2^{\pm}$ exist below; for $\mathrm{Re}(c) < 0$, the saddle point p_1 lies on the negative real axis for $(\mathrm{Re}(c), \lambda)$ above FB^1 and on the positive real line below it. The curve FB^1 emanates from the centre C_1, which is also the starting point of another curve of forward-backward critical tangencies, labelled FB^2 (green). This is the curve of forward-backward critical tangencies between J_2 and J_0. The period-two attractors $q_2^{\pm}$ and $r_2^{\pm}$ exist for $(\mathrm{Re}(c), \lambda)$ above the curve FB^2 and the period-four saddles p_4^k, $1 \leq k \leq 4$, exist below it.

Three further bifurcation curves emanate from the point C_1: the curve PF^1 (blue) of pitchfork bifurcations of p_1, the curve PD^1 (magenta) of period-doubling bifurcations of p_1, and the curve PF^2 (blue) of pitchfork bifurcations of $p_2^{\pm}$. The curve PF^1, to the right of C_1, corresponds to the orientation-preserving case. The point p_1 is an attractor for $(\mathrm{Re}(c), \lambda)$ above PF^1 and a saddle below it, and the two period-two attractors $q_1^{\pm}$ exist only below PF^1. The curves PD^1 and PF^2, to the left of C^1, correspond to the orientation-reversing case. For $(\mathrm{Re}(c), \lambda)$ above PD^1, the point p_1 is an attractor, and below PD^1 it is a saddle; between PD^1 and PF^2, the period-two points $p_2^{\pm}$ are attractors, and below PF^2, they are saddles; and the period-two attractors $q_2^{\pm}$ and $r_2^{\pm}$ exist only below PF^2.

The curve PF^1 ends at the point S_1 to the right of C_1. Two further bifurcation curves emanate from S_1; these are the curve NS^1 (red) of Neimarck–Sacker bifurcations of $q_1^{\pm}$ and the curve L^1 (black) of saddle-node bifurcation of p_1 and s_1. The points $q_1^{\pm}$ are repellors for $(\mathrm{Re}(c), \lambda)$ to the right of NS^1 and attractors to its left. The curve NS^1 seems to be tangent to the curve FB^1 at $(\mathrm{Re}(c), \lambda) = (0.5, 0.5)$, but, in fact, NS^1 consists of two segments that end in points on FB^1 very close to $(0.5, 0.5)$. The curve L^1 is given analytically by $\{(\mathrm{Re}(c), \lambda) : \lambda = (1 + \mathrm{Re}(c) \pm \sqrt{\mathrm{Re}(c)(\mathrm{Re}(c) + 2)})/2\}$ and has asymptote $\lambda = 0$ as $\mathrm{Re}(c) \to \infty$. The fixed points p_1 and s_1 exist only for $(\mathrm{Re}(c), \lambda)$ to the left of L^1. The curve NS^1 always appears to stay above L^1 and also goes to $\lambda = 0$ for $\mathrm{Re}(c) \to \infty$ (not shown).

The curve PD^1 ends at the point P_1 to the left of C_1. One further bifurcation curve emanates from P_1, namely, the curve NS^2 (red) of Neimarck–Sacker bifurcations of the symmetric period-two points $q_2^{\pm}$ and $r_2^{\pm}$. The points $q_2^{\pm}$ and $r_2^{\pm}$ are attractors for $(\mathrm{Re}(c), \lambda)$ below NS^2 and repellors above. As for NS^1 and FB^1, the curve NS^2 seems to be tangent to FB^2, but, in fact, it consists of two segments that end at two points on FB^2 which lie very close together. The right segment of NS^2 and the curve PF^2 both end at the same point on the curve L^2 (black) of saddle-node bifurcations of $p_2^{\pm}$ and $s_2^{\pm}$. The curve L^2 emerges from a point on the curve PD^1; it is given analytically by $\{(\mathrm{Re}(c), \lambda) : \lambda = (2 - \mathrm{Re}(c) \pm 2\sqrt{-\mathrm{Re}(c)})/(\mathrm{Re}(c)^2 + 4)\}$ and has asymptote $\lambda = 0$ for $\mathrm{Re}(c) \to -\infty$. Note that the curves L^1 and L^2 are tangent to each other at the point $(\mathrm{Re}(c), \lambda) = (0, 0.5)$, which is the transcritical bifurcation of all saddle and repelling periodic points for $c = 0$; see Section 3.1.

Close to the two intersection points of the curves L^1 and FB^1, we find the curves H^0 (magenta) of first homoclinic and B^0 (red) of first backward critical tangencies of p_1. The unstable set $W^u(p_1)$ has a homoclinic

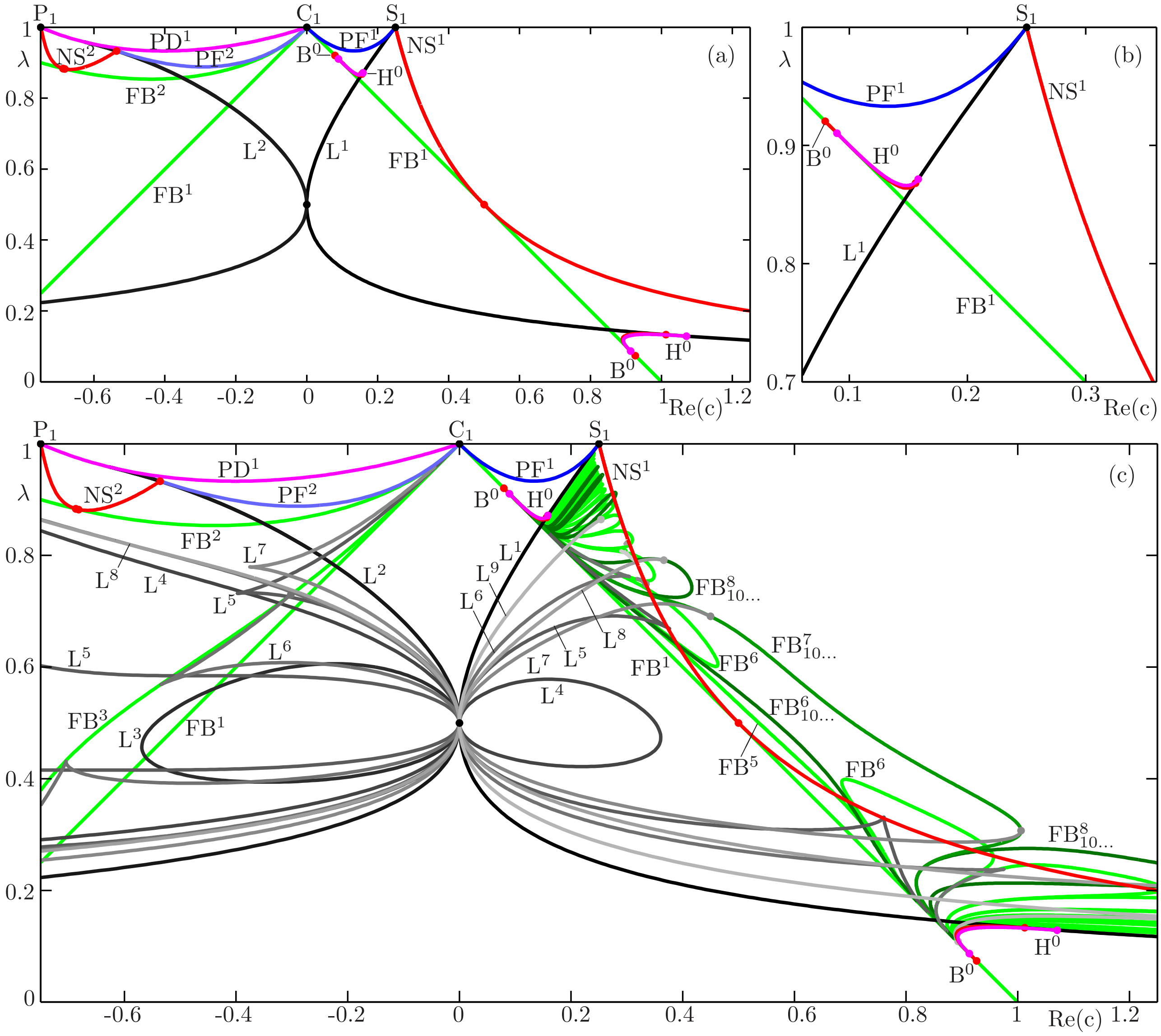

Figure 13: The bifurcation diagram of (1) in the $(\mathrm{Re}(c), \lambda)$-plane for $\mathrm{Im}(c) = 0$. The points S_1, C_1 and P_1 for $\lambda = 1$ are the right boundary, the centre and the left boundary of the main cardioid of the Mandelbrot set $\mathcal{M}$, respectively. Panel (a) shows the main bifurcations of the fixed points p_1 and $q_1^{\pm}$, the period-two points $p_2^{\pm}$ and $q_2^{\pm}$, and the circles J_1 and J_2; these are the period-doubling bifurcation PD^1 (magenta) of p_1; the pitchfork bifurcations PF^1 and PF^2 (blue) of p_1 and $p_2^{\pm}$, respectively; the saddle-node bifurcations L^1 and L^2 (black) of p_1 and $p_2^{\pm}$ with s_1 and $s_2^{\pm}$, respectively; the Neimarck–Sacker bifurcations NS^1 and NS^2 (red) of $q_1^{\pm}$, $q_2^{\pm}$ and $r_2^{\pm}$, respectively; the first homoclinic tangency H^0 (magenta) of p_1; the first backward critical tangency B^0 (red) of p_1; and the forward-backward critical tangencies FB^1 and FB^2 (green) of J_1 and J_2, respectively. Panel (b) is an enlargement of the bifurcation diagram in panel (a). Panel (c) shows, in addition, the curves of saddle-node bifurcations L^k (black) of period-k points for $3 \leq k \leq 9$ and of forward-backward critical tangencies FB^k (green) and $\mathrm{FB}^k_{10\ldots}$ (dark green).

tangle with the stable set $W^s(p_1)$ between H^0 and L^1, and $W^u(p_1)$ has self-intersections between B^0 and L^1. An enlargement of these curves for $\lambda > 0.5$ is shown in Figure 13(b). Note that B^0 lies between H^0 and L^1.

Numerically, we found that the curves H^0 and B^0 each connect a point on FB^1 to a point on L^1.

Figure 13(c) shows, in addition, the curves L^k (grey), $3 \leq k \leq 9$, of saddle-node bifurcations of period-k saddle and repelling periodic orbits. These curves are all tangent to each other at the point $(\mathrm{Re}(c), \lambda) = (0, 0.5)$ and, hence, this point acts as an organising centre for the dynamics of (1). Panel (c) also shows more curves of forward-backward critical tangencies of the critical point J_0 with curves $J_k \subset \mathcal{J}^+$ for some k with $3 \leq k \leq 50$. The curves FB^k (green) denote forward-backward critical tangencies between J_k and J_0 that correspond to forward-backward critical tangencies between J_1 and $J^{0\ldots 0}_{-(k-1)}$. The curves $\mathrm{FB}^k_{10\ldots}$ (dark green) denote forward-backward critical tangencies between J_k and J_0 that correspond to forward-backward critical tangencies between J_1 and $J^{10\ldots 0}_{-(k-1)}$. The curves FB^k and $\mathrm{FB}^k_{10\ldots}$ form a complicated structure of closed curves that all appear to emerge from the point C_1 for $\lambda \geq 0.5$ and the point $(\mathrm{Re}(c), \lambda) = (1, 0)$ for $\lambda \leq 0.5$. Both sequences FB^k and $\mathrm{FB}^k_{10\ldots}$ accumulate on the curves B^0 of first backward critical tangencies; however, here, they also accumulate on L^1 to the right of the end points of H^0 on L^1; see also already Figure 14(a).

Overall, we see that the bifurcation diagram in Figure 13 reflects the transitions for decreasing $\lambda \in [0, 1]$ for the four cases of c we discussed in Sections 3 and 4. The case $c = 0$ starting at the centre C_1 of $\mathcal{M}$ is highly degenerate, in the sense that the chaotic attractor $\mathcal{A}$ is created at once for $\lambda < 1$ and that the transcritical bifurcation at $(\mathrm{Re}(c), \lambda) = (0, 0.5)$ is an organising centre that gives rise to infinitely many saddle-node bifurcations. The case $c = 0.1$ represents the orientation-preserving case for $c \in (0, 0.25)$ in the following sense: for decreasing λ from 1, the attractor p_1 becomes the first saddle point in the pitchfork bifurcation PF^1, the attractors $q_1^\pm$ turn into the period-two saddle points $p_2^\pm$ in the last forward-backward critical tangency FB^1 and p_1 disappears at the saddle-node bifurcation L^1; on the way, an infinite sequence of forward-backward critical tangencies (including FB^k and $\mathrm{FB}^k_{10\ldots}$) is passed leading to the appearance of infinitely many saddle periodic points; finally, the saddle point p_1 reappears at the saddle-node bifurcation L^1; compare with the transition in Figures 3, 5 and 7. Similarly, the case $c = -0.25$ represents the orientation-reversing case for $c \in (-0.75, 0)$ in the following sense: for decreasing λ from 1, the attractor p_1 becomes the first saddle point in the period-doubling bifurcation PD^1, which is followed by either the pitchfork bifurcation PF^2, where $p_2^\pm$ become the first period-two saddles, or by the Neimarck–Sacker bifurcation NS^2, where $q_2^\pm$ and $r_2^\pm$ turn into attractors; the points $q_2^\pm$ and $r_2^\pm$ turn into the period-four saddle points p_4^k, $1 \leq k \leq 4$, in the forward-backward critical tangency FB^2 and $p_2^\pm$ disappear at the saddle-node bifurcation L^2; as for $c = 0.1$, we pass an infinite sequence of forward-backward critical tangencies leading to the appearance of infinitely many saddle periodic points (not shown); the saddle point p_1 moves over J_0 in the last forward-backward critical tangency FB^1; finally, the period-two saddle points $p_2^\pm$ reappear at the saddle-node bifurcation L^2; compare with the transition in Figures 8 and 9. For $c \notin \mathcal{M}$, we find two fundamentally different cases. The case $c = 0.28$ represents the orientation-preserving case for $c \in (0.25, 1)$ in the following sense: for decreasing λ from 1, an infinite sequence of forward-backward critical tangencies is passed, which we believe accumulates on the first interaction of the Julia set $\mathcal{Y}$ and $\mathcal{J}^+$; the fixed points $q_1^\pm$ become the first attractors in this transition at the Neimarck–Sacker bifurcation NS^1; they turn into period-two saddle points $p_2^\pm$ at the last forward-backward critical tangency FB^1; finally, the first saddle fixed point appears at the saddle-node bifurcation L^1; compare with the transition in Figures 10 and 12. For fixed $c > 1$ and decreasing λ from 1, map (1) initially undergoes the same transition as for $c \notin \mathcal{M}$ and $c < 1$, but it does not pass the last forward-backward critical tangency FB^1 and, hence, the repellors $q_1^\pm$ persist until $\lambda = 0$.

The saddle-node bifurcation L^1, the last forward-backward critical tangency FB^1 and the Neimark-Sacker bifurcation NS^1 are the main bifurcations involved in the topological changes of the Julia set $\mathcal{Y}$ in the phase space for $c > 0$, as discussed in Sections 3.2 and 4.1. To understand how they relate to each other and to other nearby bifurcations, we show in Figure 14 four enlargements of the bifurcation diagram in Figure 13(c) near L^1, FB^1 and NS^1. Figure 14(a) is an enlargement showing that the curves FB^k and $\mathrm{FB}^k_{10\ldots}$ of forward-backward critical tangencies accumulate on the curve B^0 of first backward critical tangencies and on the curve L^1 of saddle-node bifurcations of p_1 and s_1 to the right of the end point of B^0 on L^1. Note that the curves $\mathrm{FB}^k_{10\ldots}$ extend further than FB^k towards the curve NS^1 and some even intersect NS^1.

Figures 14(b)–(d) are three enlargements along the curve NS^1 showing curves L^8, L^{15} and L^7 of saddle-node bifurcations of periodic points of periods 8, 15 and 7, respectively. These curves form resonance tongues that start at the resonance points on NS^1 with rotation numbers $1/8 < 2/15 < 1/7$, that is, where the fixed points $q_1^\pm$ have eigenvalues $\exp(i2\pi p/q)$ for $p/q = 1/8$, $2/15$ and $1/7$, respectively. The curves L^8, L^{15} and L^7 each consist

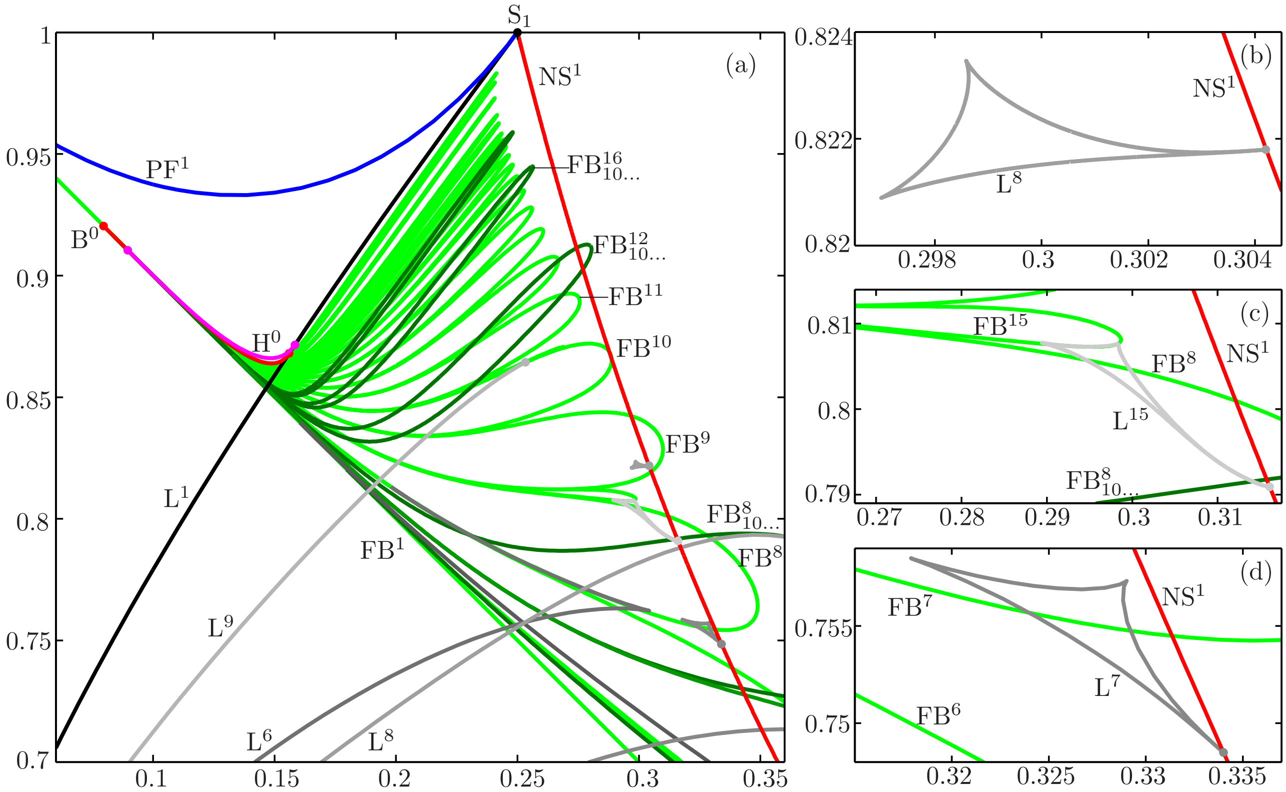

Figure 14: The bifurcation diagram of (1) in the $(\mathrm{Re}(c), \lambda)$-plane for $\mathrm{Im}(c) = 0$. Panel (a) is an enlargement of the bifurcation diagram in Figure 2(c) near the curves NS^1, PF^1 and FB^1. Panels (b)–(d) are enlargements of the bifurcation diagram in panel (a) near regions of 1:8, 2:15 and 1:7 resonances.

of three segments connected at three cusp points, where one of them is the corresponding resonance point on NS^1. The two segments that connect at these resonance points on NS^1 correspond to saddle-node bifurcations of a repelling and a saddle orbit of the corresponding periods, which form an invariant circle with phase locking around $q_1^{\pm}$ for $(\mathrm{Re}(c), \lambda)$ inside these resonance tongues. The middle segments (opposite the resonance points on NS^1) correspond to saddle-node bifurcations of the repelling orbit with another saddle periodic orbit that is not on the invariant circle. Note that the curves L^7 and L^{15} intersect the curves FB^7 and FB^{15} of forward-backward critical tangencies. At the bifurcations FB^7 and FB^{15}, the 7-periodic or 15-periodic saddle orbit that does not lie on the invariant circle moves over J_0 and a sequence of its preimages in phase space. This bifurcation is similar to FB^1 for $\mathrm{Re}(c) < 0$ in Figure 13(a), where the saddle point p_1 lies to the left of J_0 for $(\mathrm{Re}(c), \lambda)$ above FB^1, and to the right of J_0 below it; compare with Figures 9(c) and (d).

5.2 Bifurcation diagram near the period-doubling sequence

Recall that the complex quadratic family (2) undergoes a sequence of period-doubling bifurcations as c is decreased along the real line and that it admits a period-three window near $\lambda = -1.75$; see Figure 1. We now investigate the bifurcation structures along the sequence of period-doubling bifurcations and the period-three window in $\mathcal{M}$. Figure 15(a) shows the bifurcation diagram of map (1) in the $(\mathrm{Re}(c), \lambda)$-plane for $(\mathrm{Re}(c), \lambda) \in [-1.38, 0.3] \times [0.84, 1]$ near the main cardioid and the bulbs of periods two and four in $\mathcal{M}$; panel (b) is an enlargement in the range $(\mathrm{Re}(c), \lambda) \in [-1.3681, -1.25] \times [0.992, 1]$ near the bulb of period four in $\mathcal{M}$; and panel (c) shows the bifurcation diagram for $(\mathrm{Re}(c), \lambda) \in [-1.76853, -1.75] \times [0.9969, 1]$ near the cardioid of period three in $\mathcal{M}$. The bifurcation structures near the period-two and four bulbs and the period-three cardioid are very similar to the bifurcation structure near the main cardioid. Along the line $\lambda = 1$ we labelled the

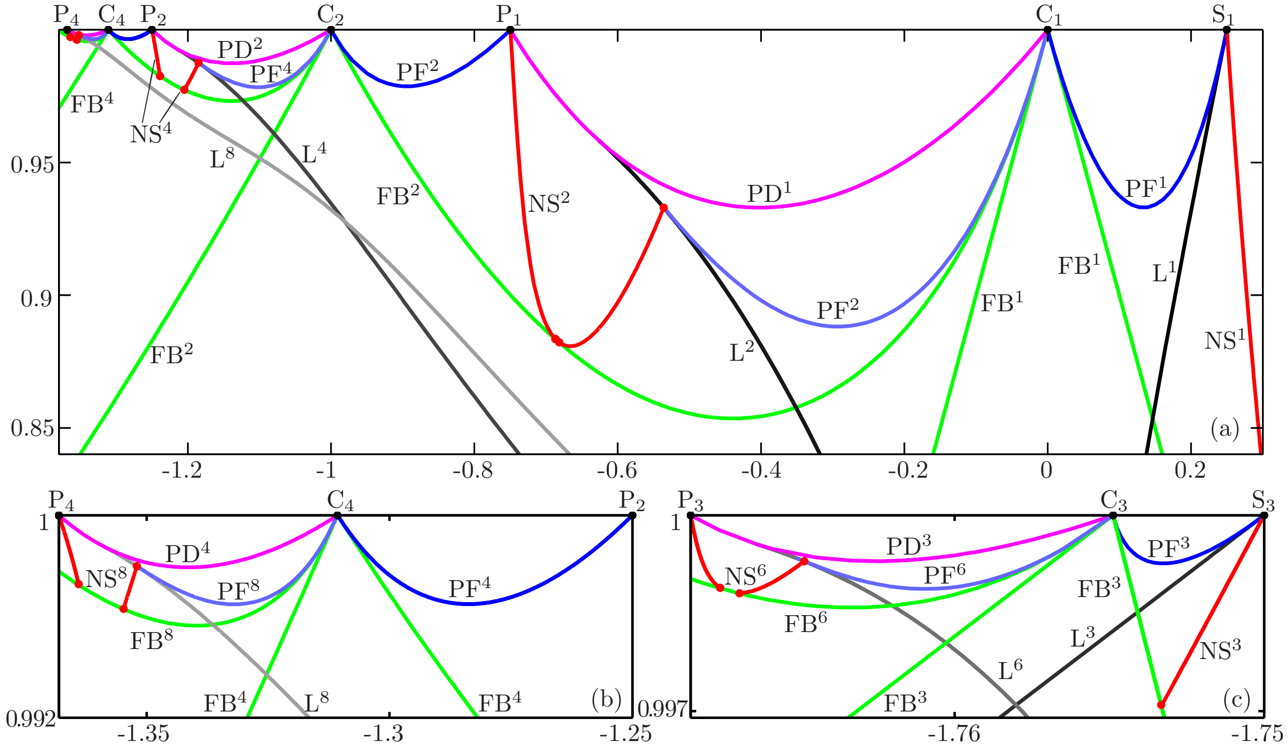

Figure 15: The bifurcation diagram of (1) in the $(\mathrm{Re}(c), \lambda)$-plane for $\mathrm{Im}(c) = 0$. Panel (a) shows the main bifurcations of the fixed points and the periodic points of periods two, four and eight near the main cardioid and the bulbs of periods two, four and eight in the Mandelbrot set $\mathcal{M}$. Panel (b) is an enlargement of the bifurcation diagram in panel (a) near the bulb of period four in $\mathcal{M}$. Panel (c) shows the main bifurcations of the periodic points of periods three and six near the cardioid of period three in $\mathcal{M}$.

following bifurcation points. As in Figure 13, the points S_1, P_1 and C_1 are the right and left boundaries and the centre of the main cardioid in $\mathcal{M} \cap \mathbb{R}$, respectively. Similarly, in Figure 15 the points $\mathrm{P}_2 = (-1.25, 1)$ and $\mathrm{P}_4 = (-1.3681, 1)$ and the points $\mathrm{C}_2 = (-1, 1)$ and $\mathrm{C}_4 = (-1.3107, 1)$ are the left boundaries and centres of the bulbs of periods two and four in $\mathcal{M} \cap \mathbb{R}$, respectively, and the points $\mathrm{S}_3 = (-1.75, 1)$, $\mathrm{P}_3 = (-1.76853, 1)$ and $\mathrm{C}_3 = (-1.754875, 1)$ are the right and left boundaries and the centre of the cardioid of period three in $\mathcal{M} \cap \mathbb{R}$, respectively; see also Figure 1. In particular, the points S_1 and S_3 are points of saddle-node bifurcations, the points P_1, P_2, P_4 and P_3 are points of period-doubling bifurcations and the points C_1, C_2, C_4 and C_3 are points, where the critical point J_0 is super-attracting, corresponding to periods one, two, four and three along the period-doubling route to chaos of (2).

In the same way as the curves FB^1, FB^2, PF^1, PF^2 and PD^1 of bifurcations of fixed and period-two points emanate from the point C_1 at the centre of the main cardioid, in Figure 15(a) the corresponding curves FB^2 and FB^4 (green) of forward-backward critical tangencies, PF^2 and PF^4 (blue) of pitchfork bifurcations and PD^2 (magenta) of period-doubling bifurcations of period-two and period-four points emanate from the point C_2 at the centre of the period-two bulb in $\mathcal{M}$; compare with Figure 13. Correspondingly, the curve L^4 (dark grey) of saddle-node bifurcations emanates from a point on PD^2, the curve NS^4 (red) of Neimarck–Sacker bifurcations emanates from P_2 and ends at a point on L^4 together with PF^4, the curve PF^2 ends at P_1 and the curve PD^2 ends at P_2. The same bifurcation structure repeats near the period-four bulb in Figure 15(b) for the curves FB^4 and FB^8 (green), PF^4 and PF^8 (blue), PD^4 (magenta), NS^8 (red) and L^8 (grey) of corresponding bifurcations of period-four and period-eight points, and near the period-three cardioid in Figure 15(c) for the curves FB^3 and FB^6 (green), PF^3 and PF^6 (blue), PD^3 (magenta), NS^6 (red) and L^6 (grey) of corresponding bifurcations of period-three and -six points. In addition, the point S^3 gives rise to the curves NS^3 and L^3 in the same way as S^1 gives rise to NS^1 and L^1.

Note that the curves L^1, L^2, L^4 and L^8 are all tangent at the point $(\mathrm{Re}(c), \lambda) = (0, 0.5)$ of transcritical bifurcation, as shown in Figure 13(c). However, the curves L^3 and L^6 in Figure 14 intersect each other transversally. Recall that NS^1 and NS^2 each consist of two segments ending on FB^1 and FB^2; see Figure 13. Similarly, in Figure 15 the curves NS^4, NS^8 and NS^6 also consist of two segments each ending on FB^4, FB^8 and FB^6. However, we were able to find only one segment of the curve NS^3, which goes from S_3 to FB^3 in Figure 15(c).

Overall, we see that the bifurcation diagram in Figure 15 has a self-similar structure that repeats along the period-doubling route to chaos on the line $\lambda = 1$, where (1) is equivalent to the complex quadratic family (2).

6 Conclusions

We studied global transitions of the dynamics of the map (1) when decreasing the parameter $\lambda \in [0, 1]$ from $\lambda = 1$, where (1) is the complex quadratic family (2), for different values of $c \in \mathbb{R}$ in the main cardioid or outside the Mandelbrot set $\mathcal{M}$. We found the tangency bifurcations from [Hittmeyer *et al.*(2013)] and, in addition, different interactions of the Julia set with the forward and backward critical sets and the stable and unstable sets of saddle fixed and periodic points of (1). These led to drastic changes of the Julia set; see Sections 3 and 4. The first saddle points are created by pitchfork, period-doubling or forward-backward critical tangency bifurcations. By following these and other critical tangency bifurcations in the two parameters $c \in \mathbb{R}$ and $\lambda \in [0, 1]$, we found that the same sequences of bifurcations occur for periodic points of higher periods along the period-doubling route to chaos on the line $\lambda = 1$.

For $\lambda = 1$ the fundamental dichotomy for the quadratic map (2) states that the Julia set $\mathcal{Y}$ is connected or totally disconnected, depending on whether the orbit of c is bounded or goes to infinity. Our numerical investigations in Sections 3–5 enable us to extend this dichotomy to $\lambda < 1$ in the following way. The topology of the Julia set $\mathcal{Y}$ of the complex quadratic map (2) persists for $\lambda < 1$ if all orbits in $\mathcal{J}^+$ behave the same, that is, if they either all stay bounded or all go to infinity. However, there is also an intermediate case, which corresponds to some orbits in $\mathcal{J}^+$ staying bounded and others going to infinity. More specifically, our careful numerical observations suggest the following three cases for $\lambda \in (0, 1)$, distinguished by properties of the basin $\mathcal{B}(\infty)$, the Julia set $\mathcal{Y}$ and the set $\mathcal{C} = \mathbb{C} \backslash (\mathcal{B}(\infty) \cup \mathcal{Y})$:

1. If all orbits in $\mathcal{J}^+$ are bounded, then $\mathcal{B}(\infty)$ is simply connected, $\mathcal{Y}$ is a connected union of Jordan curves, there is at least one finite (periodic or chaotic) attractor, and $\mathcal{C}$ is not empty; see Figures 2(a)–(e), 3, 5(a)–(c), 7(c)–(e), 8, 9(a)–(b) and (f)–(h), and 12(e)–(f).

2. If all orbits in $\mathcal{J}^+$ go to infinity, then $\mathcal{B}(\infty)$ is connected, but not simply connected, $\mathcal{Y}$ is a Cantor set, and $\mathcal{C}$ is empty; see Figures 10(a)–(c).

3. If some orbits in $\mathcal{J}^+$ stay bounded and other orbits in $\mathcal{J}^+$ go to infinity, we find three different scenarios:

   (a) If there is no finite attractor and J_0 lies in the disk bounded by J_1, then $\mathcal{C}$ is empty, $\mathcal{B}(\infty)$ is simply connected, and $\mathcal{Y}$ is a Cantor bouquet with explosion point J_0; see Figures 5(d)–(f), 7(a)–(b), 9(d)–(e) and 12(c)–(d).

   (b) If there is no finite attractor and J_0 lies outside the disk bounded by J_1, then $\mathcal{C}$ is empty, $\mathcal{B}(\infty)$ is not connected, but consists of a countably infinite number of components, and $\mathcal{Y}$ is a Cantor tangle, that is, similar to a Cantor bouquet, but with the dense set $\mathcal{J}^-$ as explosion points; $\mathcal{Y}$ has infinitely many "holes", which are given by the bounded components of $\mathcal{B}(\infty)$; see Figures 9(c) and 10(d)–(e).

   (c) If there is at least one finite hyperbolic attractor, then $\mathcal{C}$ is not empty and $\mathcal{B}(\infty)$ is not connected; both $\mathcal{C}$ and $\mathcal{B}(\infty)$ consist of a countably infinite number of components; $\mathcal{Y}$ is a Cantor cheese with the dense set $\mathcal{J}^-$ as explosion points, that is, it is effectively a Cantor tangle with infinitely many additional "holes" given by the components of $\mathcal{C}$; see Figures 10(f) and 12(a).

In the transitions of the map (1) away from the complex quadratic family (2), we found the first example of a nonanalytic map with a Julia set that is a Cantor bouquet. In particular, this Cantor bouquet has a finite explosion point, whereas the examples in the literature, such as the exponential function $z \mapsto \lambda \exp(z)$, have infinity as the explosion point [Aarts & Oversteegen(1993), Bula & Oversteegen(1990), Devaney & Krych(1984), Krauskopf & Kriete(1998), Mayer(1990)]. Furthermore, we find two other types of interesting Julia sets, which we called the Cantor tangle and the Cantor cheese. These sets have complicated topological structures, which need further analytical and numerical analysis to be fully understood. In particular, these three types of Julia sets have in common that they are given by the closure of stable sets of saddle fixed and periodic points of the map; this is impossible for Julia sets in complex analytic maps, but seems to be a new phenomenon specific to this type of nonanalytic map. The perturbation of the two-dimensional quadratic map considered in [Romero *et al.*(2009)] also admits a Julia set that is given by the closure of the stable set of a saddle point, but the unperturbed map is already nonanalytic; further research is necessary to determine if this Julia set shares other properties with the Cantor bouquet, Cantor tangle or Cantor cheese we found in the map (1).

We only considered real c, but we expect to find a similar bifurcation structure if c has a small imaginary part. More specifically, we expect the last forward-backward critical tangency to become one smooth curve, the pitchfork bifurcations to turn into saddle node bifurcations and the curves of homoclinic tangencies, backward critical tangencies and Neimarck–Sacker bifurcations to split up in two curves each. Furthermore, for a fixed nonzero imaginary part of c, there is no longer a super-attracting case and the points of saddle-node and period-doubling bifurcations on the boundary of the Mandelbrot set are replaced by other points on the boundary. Therefore, we expect that the end points of the bifurcation curves that lie in the interior of the Mandelbrot set for $c \in \mathbb{R}$ move away from the line $\lambda = 1$ as the imaginary part of c is increased, and that other bifurcation curves emanate from the boundary of the Mandelbrot set. Further research is needed to understand how these curves connect with each other, and how this relates to the complicated bifurcation scenarios on the boundary of the Mandelbrot set.

Recall that, for $a \in (0, 1)$ and $c = 1$, the map (3) was constructed in [Bamón *et al.*(2006)] as the reduction of a Lorenz-like attractor in an n-dimensional vector field for $n \geq 5$. The homoclinic, forward critical, backward critical and forward-backward critical tangencies of (3), which organise its transition to wild chaos, correspond to homoclinic and heteroclinic bifurcations of an equilibrium and a periodic orbit in the vector field. In the construction of the map (3), the parameter a is defined as $a := -\lambda_2/\lambda_3$, where $\lambda_2 < 0$ is the weak stable eigenvalue and λ_3 is the unstable eigenvalue of the equilibrium in the underlying vector field. One of the conditions of the Lorenz-like attractor is that the attractor is expanding, that is, $a < 1$. Therefore, if $a = 2$, the map (3) no longer corresponds to a Lorenz-like attractor, but to a so-called *contracting Lorenz attractor* or *Rovella-like attractor*; see [Keller & Pierre(2001), Rovella(1993)] for studies in three-dimensional vector fields and [Araújo *et al.*(2011)] for a higher-dimensional analogue. These are singular attractors that can be reduced to a one- or two-dimensional noninvertible map in the same way as the geometric Lorenz attractor or higher-dimensional Lorenz-like attractors, respectively, but that are contracting instead of expanding.

In [Hittmeyer *et al.*(2013)] we concluded that the map (3) exhibits wild chaos in the $(\text{Re}(c), \lambda)$-plane for fixed $a = 0.8$ and $\text{Im}(c) = 0$ between the first backward critical tangency, the last forward-backward critical tangency and the line $\lambda = 1$. Therefore, for $a = 2$ in the map (3), the geometric ingredients for wild chaos appear to be present in the two regions between the first backward critical tangency, the last forward-backward critical tangency and the saddle-node bifurcation of the fixed point (see Figure 13) and corresponding regions near the other bulbs and cardioids in the Mandelbrot set $\mathcal{M}$. One of the assumptions in the proof of existence of wild chaos in [Bamón *et al.*(2006)] is that the map (3) is area-expanding in a neighbourhood of the attractor. For $a \in (0, 1)$ the map (3) has unbounded derivative near J_0 and, therefore, it is area-expanding on a subset of the attractor after the first backward critical tangency. In [Hittmeyer *et al.*(2013)] we conjectured that this partial area-expansiveness on a large subset of the attractor is sufficient for the existence of wild chaos. However, for $a = 2$ the map (3) no longer has unbounded derivative near the critical point and, hence, it is not necessarily area-expanding in a neighbourhood of this point. However, we can find a neighbourhood of the intersection point of the curves of last forward-backward critical tangencies and saddle-node bifurcations in the $(\text{Re}(c), \lambda)$-plane, in which (3) is area-expanding at the saddle fixed point p_1. Although it is unclear to us if the arguments from the proof of existence of wild chaos in [Bamón *et al.*(2006)] can be extended to this parameter regime, our numerical evidence suggests the existence of complicated dynamics in this parameter regime, and we conjecture the existence of a wild Rovella-like attractor in this regime.

In future research, we also plan to investigate the connection between the regime near the complex quadratic family for $a = 2$ in map (3) and the regime of wild chaos for $a < 1$. Bielefeld et al. [(1993)] and Bruin and van Noort [(2004)] already give us information on this connection for fixed $\lambda = 1$ and $a \in (1, 2)$. They found attracting periodic points that do not attract the critical orbit and they found curves of Neimarck–Sacker, saddle-node, period-doubling and heteroclinic tangency bifurcations. However, for $\lambda < 1$, the dynamics of (3) is more complicated, because the critical value c gets perturbed to the critical circle J_1 and, therefore, admits infinitely many critical orbits. This allows for more different scenarios of complicated dynamics, such as forward-backward critical tangencies and the intermediate cases, where some critical orbits go to infinity and other critical orbits stay bounded. Moreover, the Julia set, which we defined as the boundary of the basin of infinity, no longer coincides with the closure of periodic and pre-periodic repelling points, because infinity is repelling. Since there are finite repelling periodic points, we expect that some parts of the Julia set go to infinity, whereas other parts stay bounded. A thorough investigation of the bifurcations of the invariant sets in the regime $a \in (0, 2]$ and $\lambda \in [0, 1]$ remains a task for future research.

Overall, we have seen in this paper that the presence of the Julia set for $a = 2$ in the map (3) allows for even more complicated bifurcations than the four tangency bifurcations. In particular, bifurcations of the Julia set in (3) correspond to additional homoclinic and heteroclinic bifurcations in the underlying vector field. More specifically, a saddle periodic point of (3) corresponds to a saddle periodic orbit with a four-dimensional stable and a two-dimensional unstable manifold in the five-dimensional vector field; see [Hittmeyer *et al.*(2013)] for more details. Similarly, a repelling periodic point of (3) corresponds to a saddle periodic orbit with a three-dimensional stable and a three-dimensional unstable manifold. Therefore, the Julia set, which is the closure of the set of periodic and pre-periodic repelling points, and the chaotic attractor, which is the closure of the set of saddle points, correspond to two hyperbolic sets with different stable and unstable dimensions; the interactions of their stable and unstable manifolds correspond to heteroclinic bifurcations in the vector field. It is yet unclear what the consequences are in the vector field when the Julia set is the closure of stable sets of saddle periodic points of the map. We expect these bifurcations to be one ingredient in the formation of so-called *heterodimensional cycles*, that is, heteroclinic cycles between these two hyperbolic sets with different stable dimensions. Wild chaos seems to play a role in the generation of (robust) heterodimensional cycles, but the exact nature of their interrelation is still an active area of research [Bonatti & Díaz(2008), Gonchenko *et al.*(2008), Shinohara(2011a), Shinohara(2011b)]. Understanding the bifurcations of the Julia set of (3) in the vector field and their role in the formation of heterodimensional cycles in more detail remains a challenging task for future research.

Another approach to investigate the interrelation between wild chaos and heterodimensional cycles is to study the vector field proposed in [Zhang *et al.*(2012)] in the same spirit. Zhang et al. developed a numerical method for the detection and continuation of heterodimensional cycles in vector fields. With this method they established the existence of a heterodimensional cycle in a four-dimensional vector field model of intracellular calcium dynamics. The advantage is that the proposed system is given by an explicit vector field. In future work we plan to study the bifurcations that occur near the detected heterodimensional cycle in this vector field. We expect that this will provide evidence for the robustness (or nonrobustness) of the existence of heterodimensional cycles in this system. Furthermore, comparing the dynamics near (robust) heterodimensional cycles in this vector field to the route to wild chaos in map (3) will give further insight into the interplay between these two phenomena.

7 Acknowledgements

The specific case $c = -0.25$ and $\lambda \in [0, 1]$ was investigated in the Master's thesis of Madeleine Jones, who was supervised at the University of Bristol by BK and SH. Her initial findings inspired our further investigation of the connections with the critical tangency bifurcations introduced in [Hittmeyer *et al.*(2013)]. We thank Bruce Peckham for fruitful discussions while he visited the University of Auckland.

References

[Aarts & Oversteegen(1993)] Aarts, J. M. & Oversteegen, L. G. [1993] "The geometry of Julia sets," *Trans. Amer. Math. Soc.* **338**, 897–918.

[Afrajmovich *et al.*(1977)] Afrajmovich, V. S., Bykov, V. V. & Shilnikov, L. P. [1977] "The origin and structure of the Lorenz attractor," *Sov. Phys. Dokl.* **22**, 253–255.

[Afrajmovich *et al.*(1983)] Afrajmovich, V. S., Bykov, V. V. & Shilnikov, L. P. [1983] "On structurally unstable attracting limit sets of Lorenz attractor type," *Trans. Mosc. Math. Soc.* **44**, 153–216.

[Araújo *et al.*(2011)] Araújo, V., Castro, A., Pacifico, M. J. & Pinheiro, V. [2011] "Multidimensional Rovella-like attractors," *J. Differ. Equations* **251**, 3163–3201.

[Back *et al.*(1992)] Back, A., Guckenheimer, J., Myers, M., Wicklin, F. & Worfolk, P. [1992] "DsTool: Computer assisted exploration of dynamical systems," *Notices Amer. Math. Soc.* **39**, 303–309.

[Bamón *et al.*(2006)] Bamón, R., Kiwi, J. & Rivera-Letelier, J. [2006] "Wild Lorenz-like attractors," arXiv 0508045, available at `http://arxiv.org/abs/math/0508045`.

[Beyn & Kleinkauf(1997)] Beyn, W.-J. & Kleinkauf, J.-M. [1997] "The numerical computation of homoclinic orbits for maps," *SIAM J. Numer. Anal.* **34**, 1207–1236.

[Bielefeld *et al.*(1993)] Bielefeld, B., Sutherland, S., Tangerman, F. & Veerman, J. J. P. [1993] "Dynamics of certain nonconformal degree-two maps of the plane," *Experiment. Math.* **2**, 281–300.

[Blanchard(1984)] Blanchard, P. [1984] "Complex analytic dynamics on the Riemann sphere," *Bull. Amer. Math. Soc.* **11**, 85–141.

[Blanchard *et al.*(2005)] Blanchard, P., Devaney, R. L., Look, D. M., Seal, P. & Shapiro, Y. [2005] "Sierpinski-curve Julia sets and singular perturbations of complex polynomials," *Ergodic Theory Dynam. Systems* **25**, 1047–1055.

[Bonatti & Díaz(2008)] Bonatti, C. & Díaz, L. [2008] "Robust heterodimensional cycles and C^1-generic dynamics," *J. Inst. Math. Jussieu* **7**, 469–525.

[Bruin & van Noort(2004)] Bruin, H. & van Noort, M. [2004] "Nonconformal perturbations of $z \mapsto z^2 + c$: the 1:3 resonance," *Nonlinearity* **17**, 765–789.

[Bula & Oversteegen(1990)] Bula, W. D. & Oversteegen, L. G. [1990] "A characterization of smooth Cantor bouquets," *Proc. Amer. Math. Soc.* **108**, 529–534.

[Carleson & Gamelin(1993)] Carleson, L. & Gamelin, T. W. [1993] *Complex dynamics*, Universitext Series (Springer-Verlag, New York).

[Devaney(2003)] Devaney, R. L. [2003] *An introduction to chaotic dynamical systems*, Studies in Nonlinearity (Westview Press, Boulder, CO).

[Devaney(2013)] Devaney, R. L. [2013] "Singular perturbations of complex polynomials," *Bull. Amer. Math. Soc.* **50**, 391–429.

[Devaney & Krych(1984)] Devaney, R. L. & Krych, M. [1984] "Dynamics of $\exp(z)$," *Ergodic Theory Dynam. Systems* **4**, 35–52.

[Dhooge *et al.*(2003)] Dhooge, A., Govaerts, W. & Kuznetsov, Yu. A. [2003] "MatCont: a Matlab package for numerical bifurcation analysis of ODEs," *ACM Trans. Math. Software* **29**, 141–164, available at `http://sourceforge.net/projects/matcont`.

[England *et al.*(2004)] England, J. P., Krauskopf, B. & Osinga, H. M. [2004] "Computing one-dimensional stable manifolds and stable sets of planar maps without the inverse," *SIAM J. Appl. Dyn. Syst.* **3**, 161–190.

[Ghaziani *et al.*(2009)] Ghaziani, R. K., Govaerts, W., Kuznetsov, Yu. A. & Meijer, H. G. E. [2009] "Numerical continuation of connecting orbits of maps in Matlab," *J. Differ. Equations Appl.* **15**, 849–875.

[Gonchenko *et al.*(2008)] Gonchenko, S. V., Shilnikov, L. P. & Turaev, D. V. [2008] "On dynamical properties of multidimensional diffeomorphisms from Newhouse regions. I," *Nonlinearity* **21**, 923–972.

[Govaerts *et al.*(2008)] Govaerts, W., Kuznetsov, Yu. A., Khoshsiar Ghaziani, R. & Meijer, H. G. E. [2008] "Cl_MatContM: a toolbox for continuation and bifurcation of cycles of maps," Software. Available at `http://sourceforge.net/projects/matcont`.

[Guckenheimer(1976)] Guckenheimer, J. [1976] "A strange, strange attractor," *The Hopf Bifurcation Theorem and its Applications*, eds. Marsden, J. E. & McCracken, M. (Springer-Verlag, New York), pp. 368–381.

[Guckenheimer & Williams(1979)] Guckenheimer, J. & Williams, R. F. [1979] "Structural stability of Lorenz attractors," *Inst. Hautes Études Sci. Publ. Math.* **50**, 59–72.

[Hittmeyer *et al.*(2013)] Hittmeyer, S., Krauskopf, B. & Osinga, H. M. [2013] "Interacting global invariant sets in a planar map model of wild chaos," *SIAM J. Appl. Dyn. Syst.* **12**, 1280–1329.

[Kaplan & Yorke(1979)] Kaplan, J. & Yorke, J. [1979] "Preturbulence: a regime observed in a fluid flow model of Lorenz," *Comm. Math. Phys.* **67**, 93–108.

[Keller & Pierre(2001)] Keller, G. & Pierre, M. [2001] "Topological and measurable dynamics of lorenz maps," *Ergodic Theory, Analysis, and Efficient Simulation of Dynamical Systems*, ed. Fiedler, B. (Springer-Verlag Berlin Heidelberg), pp. 333–361.

[Krauskopf & Kriete(1998)] Krauskopf, B. & Kriete, H. [1998] "Approximating transcendental Julia sets," *Progress in holomorphic dynamics*, ed. Kriete, H. (Longman, Harlow), pp. 116–138.

[Krauskopf & Osinga(1998)] Krauskopf, B. & Osinga, H. [1998] "Growing 1D and quasi-2D unstable manifolds of maps," *J. Comput. Phys.* **146**, 404–419.

[Krauskopf & Osinga(2000)] Krauskopf, B. & Osinga, H. [2000] "Investigating torus bifurcations in the forced Van der Pol oscillator," *Numerical Methods for Bifurcation Problems and Large-Scale Dynamical Systems (Minneapolis, MN, 1997)* (Springer-Verlag, New York), pp. 199–208.

[Marotta(2008)] Marotta, S. M. [2008] "Singular perturbations in the quadratic family," *J. Difference Equ. Appl.* **14**, 581–595.

[Mayer(1990)] Mayer, J. C. [1990] "An explosion point for the set of endpoints of the Julia set of $\lambda \exp(z)$," *Ergodic Theory Dynam. Systems* **10**, 177–183.

[McDonald *et al.*(1985a)] McDonald, S. W., Grebogi, C., Ott, E. & Yorke, J. A. [1985a] "Fractal basin boundaries," *Phys. D* **17**, 125–153.

[McDonald *et al.*(1985b)] McDonald, S. W., Grebogi, C., Ott, E. & Yorke, J. A. [1985b] "Structure and crises of fractal basin boundaries," *Phys. Lett. A* **107**, 51–54.

[McMullen(1988)] McMullen, C. [1988] "Automorphisms of rational maps," *Holomorphic functions and moduli, Vol. I (Berkeley, CA, 1986)*, eds. Drasin, D., Kra, I., Earle, C., Marden, A. & Gehring, F. (Springer-Verlag, New York), pp. 31–60.

[Milnor(2006)] Milnor, J. [2006] *Dynamics in one complex variable*, Annals of Mathematics Studies, Vol. 160, 3rd ed. (Princeton University Press, Princeton, NJ).

[Mira *et al.*(1996)] Mira, C., Gardini, L., Barugola, A. & Cathala, J.-C. [1996] *Chaotic Dynamics in Two-Dimensional Noninvertible Maps*, World Sci. Ser. Nonlinear Sci. Ser. A Monogr. Treatises, Vol. 20 (World Scientific, Singapore).

[Osinga *et al.*(2013)] Osinga, H. M., Krauskopf, B. & Hittmeyer, S. [2013] "Chaos and wild chaos in Lorenz-type systems," Preprint, The University of Auckland.

[Palis & de Melo(1982)] Palis, J. & de Melo, W. [1982] *Geometric Theory of Dynamical Systems* (Springer-Verlag, New York).

[Peckham(1998)] Peckham, B. B. [1998] “Real perturbation of complex analytic families: points to regions,” *Internat. J. Bifur. Chaos Appl. Sci. Engrg.* **8**, 73–93.

[Peckham & Montaldi(2000)] Peckham, B. B. & Montaldi, J. [2000] “Real continuation from the complex quadratic family: fixed-point bifurcation sets,” *Internat. J. Bifur. Chaos Appl. Sci. Engrg.* **10**, 391–414.

[Romero *et al.*(2009)] Romero, N., Rovella, A. & Vilamajó, F. [2009] “Perturbations of the quadratic family of order two: the boundary of hyperbolicity,” *Nonlinearity* **22**, 1145–1165.

[Rovella(1993)] Rovella, A. [1993] “The dynamics of perturbations of the contracting Lorenz attractor,” *Bol. Soc. Brasil. Mat.* **24**, 233–259.

[Shinohara(2011a)] Shinohara, K. [2011a] “An example of C^1-generically wild homoclinic classes with index deficiency,” *Nonlinearity* **24**, 1961–1974.

[Shinohara(2011b)] Shinohara, K. [2011b] “On the index problem of C^1-generic wild homoclinic classes in dimension three,” *Discrete Contin. Dyn. Syst. Ser. A* **31**, 913–940.

[Zhang *et al.*(2012)] Zhang, W., Krauskopf, B. & Kirk, V. [2012] “How to find a codimension-one heteroclinic cycle between two periodic orbits,” *Discrete Contin. Dyn. Syst. Ser. A* **32**, 2825–2851.